
PLASMA
DYNAMICS

Dynamics of Heterogeneous Liners with Prolonged Plasma Creation

V. V. Aleksandrov¹, A. V. Branitskii¹, G. S. Volkov¹, E. V. Grabovskii¹, M. V. Zurin¹,
S. L. Nedoseev¹, G. M. Oleinik¹, A. A. Samokhin¹, P. V. Sasorov^{1,2}, V. P. Smirnov¹,
M. V. Fedulov¹, and I. N. Frolov¹

¹Troitsk Institute for Innovation and Thermonuclear Research, Troitsk, Moscow oblast, 142092 Russia

²Institute of Theoretical and Experimental Physics, Bol'shaya Cheredushinskaya ul. 25, Moscow, 117259 Russia

Received May 23, 2000

Abstract—Prolonged plasma creation in heterogeneous liners, in which the liner substance is separated into two phase states (a hot plasma and a cold skeleton), is investigated both experimentally and theoretically. This situation is typical of multiwire, foam, and even gas liners in high-current high-voltage facilities. The main mechanisms governing the rate at which the plasma is created are investigated, and the simplest estimates of the creation rate are presented. It is found that, during prolonged plasma creation, the electric current flows through the entire cross section of the produced plasma shell, whose thickness is comparable with the liner radius; in other words, a current skin layer does not form. During compression, such a shell is fairly stable because of its relatively high resilience. It is shown that, under certain conditions, even a thick plasma shell can be highly compressed toward the discharge axis. A simplified numerical simulation of the compression of a plasma shell in a liner with prolonged plasma creation is employed in order to determine the conditions for achieving regimes of fairly compact and relatively stable radial compression of the shell. © 2001 MAIK “Nauka/Interperiodica”.

1. INTRODUCTION

In recent years, significant progress has been achieved in generating high-power X-ray pulses in high-current high-voltage Z-pinch facilities [1, 2]. This progress has been made possible due to the implementation of the idea [3] of optimized radial collapse of a light liner onto a central target (the so-called double-liner scheme) under conditions typical of facilities with sufficiently high currents (such as Saturn and Z), when the light liner can be composed of many (up to 200–300) thin metal wires. Specifically, in the Z facility at Sandia National Laboratory (USA) [2], a 20-MA current with a rise time of 105 ns was switched on to a 2-cm-long and 4-cm-diameter cylindrical multiwire liner composed of 240 tungsten wires, each having a diameter of 7.5 μm . In a series of experiments carried out without a central target, 2-MJ X-ray pulses with a peak intensity of 200 TW and a full width at half-maximum (FWHM) of 5.5 ns were generated at the time at which the liner collapsed onto the discharge axis. One of the most important results obtained in those experiments was that of achieving such a relation between the current rise time and the FWHM of the generated X-ray pulse.

These experimental results motivated investigations of inertial confinement fusion (ICF) in Z-pinch facilities, the more so since facilities of this type are less expensive in comparison with, e.g., facilities for laser-driven ICF. Further progress in this field requires that

the power of an X-ray pulse be made several times higher; such X-ray pulses could in principle be generated in machines that would be capable of operating with current pulses two to three times higher. Following from this, the question arises of how to scale the results obtained previously. To answer this question and, accordingly, to optimize the liner design and parameters, we must find the physical factors that govern such a symmetric and compact compression of multiwire liners in comparison with, e.g., gas liners with similar parameters [4, 5]. The renewed interest in the physical research on the compression of multiwire liners was a reaction to these important issues [6–14].

The main (and still undoubted) point in interpreting experimental data is that the multiwire structure of a liner leads to the compact compression of the produced plasma shell, thereby ensuring high densities of the kinetic and magnetic energies of the liner near the system axis. In attempting to explain such a compact compression of the plasma shell produced in a multiwire liner, most of the authors [6–13] assumed that a continuous cylindrical plasma shell with a fairly high degree of axial symmetry is formed on a sufficiently short time scale. According to this approach, it is the high symmetry of the produced plasma shell that ensures the symmetry and compactness of the liner plasma implosion and is responsible for the delayed onset of the Rayleigh–Taylor (RT) instability. In this case, the governing parameter of a multiwire liner is the ratio of the interwire gap to the diameter of the current-carrying

plasma cylinder produced by an electric explosion of each individual wire [6, 11].

This paper is devoted to the experimental and theoretical justification of another approach to interpreting efficient compression of plasma shells formed in multiwire liners. We do not deny the importance of the symmetry of the initial state of a plasma liner, assuming, however, that it plays a secondary role. Our approach provides other ways of optimizing the compact compression of plasma liners.

The essence of our approach can be briefly described as follows. Multiwire liners ensure much more stable distributions of the produced current-carrying plasma in comparison with those in gas liners. This stems from both the heterogeneous nature of the liner (the presence of a hot plasma, which carries the main plasma current, and a relatively cold substance, which is produced directly by the electric explosions of the wires) and the associated prolonged plasma creation. Below, the term “plasma creation” does not mean a conventional ionization process but refers to the production of a plasma whose conduction is high enough for it to carry the bulk of the generator current and whose ohmic resistance is lower than the internal resistance of the generator and is comparable to or even lower than the impedance related to the change in the inductance of the liner. During prolonged plasma creation, the produced current-carrying plasma converges continuously toward the system axis, thereby giving rise to a plasma shell whose thickness is markedly larger than the skin depth, the magnetic field and current being, however, nonzero over the entire cross section of the shell. At the initial stages of compression, the plasma shell may even be discontinuous in the azimuthal direction. The convergence of a thick plasma shell toward the system axis is ensured by the spatially distributed Ampère force $j \times B/c$, which is almost uniform over the entire cross section of the shell, rather than by a magnetic piston, which acts on the outer surface of the liner and gives rise to strong instabilities. Such plasma liners are much less subjected to the RT instability as compared to thin plasma shells of thicknesses comparable to the skin depth.

At the same time, the plasma shell resilience caused by the frozen-in magnetic field may reduce the extent of radial compression. Obviously, there exists an optimum shell thickness that is small enough to ensure sufficiently compact compression, as if the instability were absent, and is large enough for the instability to be suppressed. We think that, in increasing the number of wires in the liner while keeping the liner mass fixed, the authors of [1, 2] groped experimentally for an optimum design for the given liner.

Here, we will not only attempt to validate some of the above assertions but also present arguments in favor of the fact that a relatively cold, thick plasma shell having a certain radial resilience caused by the frozen-in magnetic field can be highly compressed toward the

system axis. In order to achieve such a high compression, the plasma pressure should be low enough and the initial current and mass densities should obey certain radial distributions. The analytic solutions presented below support this conclusion and disprove the widely accepted opinion that thick resilient plasma shells cannot be compressed effectively. Our results provide new ways of optimizing the design of multiwire liners.

The high-power pulsed electric energy sources in which we are interested here were designed and built in the 1970s with the purpose of generating megaampere relativistic electron beams with a duration of several tens of nanoseconds. Such generators were later used, in particular, to supply fast self-compressed plasma discharges. As a result, a qualitatively new situation arose that had never been encountered in classical megaampere Z-pinch and microsecond plasma foci. The essential features of this situation can be explained as follows. The requirement that the pinch compression rate be consistent with the much faster rise time of the discharge current necessitated a proportional (other conditions being the same) decrease in the initial pinch radius (to approximately one centimeter). Accordingly, the initial density of the plasma-producing substance to be compressed was increased by a factor of several tens or even several hundreds. Consequently, fundamentally new methods were developed to create substances with the desired initial density distributions. As a result, the final parameters of a compressed fast Z-pinch were found to depend critically on its initial shape and other characteristics. This is an important feature in which fast Z-pinch devices differ from plasma focus devices and which makes it possible to carry out experiments with fast pinches of complicated initial shapes, unachievable in classical devices [3, 15, 16], and subsequently with pinches whose heterogeneous substance contains a condensed plasma-producing component [1, 17, 18].

It was found that, under the “cold start” conditions of a fast pinch (when the plasma is created by the discharge current itself), the plasma creation process is spatially nonuniform. Using as an example foam and gas liners, Branitskiĭ *et al.* [18] thoroughly analyzed the cold-start effects, which result in nonuniform plasma creation in fast superterawatt self-compressed discharges. In gas liners, the appearance of a hot plasma component in an initial, almost uniform, cold substance most likely stems from thermal and ionization instabilities, which lead to plasma filamentation at the very beginning of the discharge. At later stages, the hot plasma component formation is probably maintained by various interchange instabilities (transverse stratification of the discharge), primarily, by the RT instability (here, we mean the second, strongly nonlinear stage of the RT instability, which was simulated in [10, 13, 19]). In foam liners, the plasma configuration is *a priori* heterogeneous because of the structure of the liner substance. Nevertheless, the filamentation and stratification instabilities peculiar to gas liners can also occur in

foam liners. Here, we are interested only in one aspect of the heterogeneous nature of plasma configurations originated from gas or foam liners; specifically, we will consider it as a cause of prolonged plasma creation—the most typical property of discharges initiated in heterogeneous plasma-producing media. In this sense, we can say that gas and foam liners resemble, to some extent, multiwire liners.

Hence, our study will cover not only multiwire liners but also other analogous heterogeneous structures, first of all, foam liners, which were thoroughly investigated by Branitskiĭ *et al.* [18]. After the discharge is initiated, “conventional” gas liners acquire a heterogeneous nature and, as was already noted, possess all of the properties of prolonged creation of a hot plasma. However, gas liners differ from multiwire and foam liners in that their heterogeneous nature stems from the onset of instabilities and, therefore, (like the plasma creation rate) is hard to control. Various heterogeneous liners can probably be classified by the extent to which their structures are regular and accordingly controllable, namely, gas, foam, and multiwire liners.

We can distinguish between the following three stages of compression of the plasma of a heterogeneous liner with prolonged plasma creation: the creation of a hot plasma, the convergence of a hot plasma toward the system axis, and the final stage of compact compression. Although our experiments were aimed at achieving the desired parameters of the compressed hot plasma at the final stage, in what follows we restrict ourselves to studying the first two stages of the dynamics of the plasma shell in a heterogeneous liner with prolonged plasma creation.

Our paper is organized as follows. In Section 2, we give a more detailed experimental and theoretical justification of the proposed scenario for compression of the plasma shell in a multiwire liner; in particular, in Section 2.2, we present new experimental data from the Angara-5-1 facility. In Section 3, we systematically describe the compression scenario. In Section 4, we theoretically examine different stages of this scenario. The most important point in our investigations is that plasma creation and plasma compression are analyzed separately. Specifically, taking into account the possibility of controlling the plasma creation process, we study the dynamics of a plasma shell in a liner with prolonged plasma creation by treating the creation rate as an independent external parameter, which is to be adjusted as necessary to optimize the compression of the shell toward the device axis. In Section 4.1, we make simple estimates of the plasma creation rate in heterogeneous plasma systems and determine how this rate depends on the current flowing through the plasma. In Section 4.2, we construct a simple model of the boundary layer near the plasma source. It is the structure of the boundary layer that governs the plasma creation rate. In Sections 4.3 and 4.4, we develop simple theoretical models of both the plasma dynamics in the

presence of a continuously operating plasma source and the compression dynamics of a thick-walled current-carrying liner. In Section 4.5, we briefly discuss the stability of compression of a thick-walled current-carrying liner. In the Conclusion, we summarize our main results.

2. REVIEW OF EXPERIMENTAL AND THEORETICAL RESULTS ON HETEROGENEOUS LINERS

2.1. Exploding Wires and Early Experiments with Multiwire Liners

In the physics of Z-pinches, heterogeneous structures with prolonged plasma creation have been known for many years. Thus, heterogeneous structures are characteristic of the simplest dense Z-pinches produced by an electric explosion of metal or dielectric wires [20–25]. In the current range 10–300 kA, thermal instabilities [21, 24, 25] cause the discharge plasma of electrically exploded wires to separate into two phase states—a hot plasma corona with a temperature of 50–200 eV, which carries essentially all of the discharge current, and a cold substance, whose density is sometimes comparable with that of solids. In this respect, the most illustrative pinch is that formed as a result of the explosion of a cryogenic deuterium fiber [22–25], when the emitted radiation plays a negligible role. In this case, the electron heat flux from the hot corona toward the cold core of the pinch causes the core to “evaporate” progressively, so that the cryogenic fiber becomes a hot plasma within a time scale of 20–100 ns (depending on both the current magnitude and wire mass [23–25]). During this process, the plasma corona tied to its source remains globally stable, despite pronounced local instabilities.

Another example of heterogeneous structures with prolonged plasma creation is multiwire liners, which have been studied for a long time (see, e.g., [26, 27]). These early experiments differed from present-day experimental investigations [1, 2] in that they were carried out with liners comprised of a relatively small number of wires (usually, from 8 to 24), because, for relatively low currents switched on to the liners, the liner mass consistent with the desired compression rate (see below) was too small (and the technology for producing thin wires was far from being perfect at the time) in order to use a large number of wires (about several hundred). Also, in early experiments, there was no need to progress in this direction. Since the distances between the wires in such liners are large enough for an exploding wire to be insignificantly affected by the other exploding wires, each individual explosion can be regarded as being essentially independent of the others and can be described by the above approach: at the initial stages of explosion, a small-mass hot plasma corona surrounds a relatively cold and dense vapor of the exploding wires, in which case the bulk of the cur-

rent should flow in the coronal plasma because of its much larger transverse cross section and much lower specific resistance (due to much higher temperatures).

An important factor originating from the multiwire nature of the liner is the collective azimuthal field \bar{B}_ϕ , which accelerates each wire toward the liner axis. If each exploding wire with the complicated heterogeneous structure described above were accelerated as a single entity, then the acceleration would be equal to $g_r = I_1 \bar{B}_\phi / (m_1 c)$, where I_1 is the current flowing in a wire and m_1 is the mass per unit length of a wire. However, for the core of the heterogeneous structure to move with such an acceleration, it should carry a current at least as high as $I_{\min} = m_1 c g_r / B_{\max}$, where $B_{\max} = 2I_1 / (R_1 c)$ is the maximum magnetic field near the outer boundary of the plasma corona formed as a result of the explosion of a wire and R_1 is the radius of the dense part of the coronal plasma. Such compression rates can be achieved under the condition

$$\frac{R_0^2 \sigma_0}{R_1^2 \sigma_1} > 2\pi \frac{R_1}{\Delta}, \quad (1)$$

where R_0 is the radius of the cold core; σ_0 and σ_1 are the conductivities of the coronal plasma and core substance, respectively; and Δ is the interwire gap. In the experiments performed up to now, this condition has not been satisfied even for $\Delta \gg R_1$, i.e., when the coronal plasma is expected to occur deep inside the regions bounded by the separatrices between the magnetic fields of the individual wires. This means that the coronal plasma accelerated toward the liner axis always remains separated from the essentially immobile exploding wire core, in which case the exploding wire substance cannot be accelerated as a whole toward the liner axis. Here, we have briefly reiterated (in the proper terminology) the analysis made by Bobrova *et al.* at the end of their paper [21],¹ which was aimed, in particular, at interpreting experiments carried out in [27]. In those experiments, it was found that the plasma “blown out” from a multiwire liner reached the discharge axis a fairly long time before the current had reached a maximum; this plasma formed a relatively stable pinch at the system axis. Then, the plasma produced by the explosions of the wires continued to flow toward the central pinch for a fairly long time after the current had reached a maximum. In [27], the properties of this radial plasma flow were studied both experimentally and theoretically. At that time, reducing the diameter of the wires while simultaneously increasing their number was not thought to be the best way of shortening the time required for the wires to become plasma and, accordingly, achieving more compact plasma shells at the final stage of radial compression of the explosion-produced plasma.

¹ This paper contains some misprints in the formulas.

2.2. Experiments on the Visualization of Prolonged Plasma Creation

In this section, we report the results of experiments with multiwire liners in the Angara-5-1 facility that provide clear evidence of the prolonged creation of a hot plasma through electric explosions of the wires. These experimental results, which were briefly described in [28], not only confirm but also significantly refine the results of earlier experiments carried out in [27] with liners comprised of a smaller number of wires. Note that the results of [27] clearly demonstrated the important role of prolonged plasma creation in multiwire liners.

Our experiments were performed with tungsten wires 6–10 μm in diameter placed along the generatrices of a cylinder 8–20 mm in diameter. The number of wires was varied from 8 to 120. The liner discharges were initiated by passing a 3–4-MA current with a rise time of 90–120 ns through the cylindrical multiwire liners. Before the main current pulse, a current prepulse heated the wires by no more than 10°C.

First, we report the results from our experiments with an 8-mm-diameter liner composed of 80 wires each having a diameter of 6 μm . Note that, since the liners in our experiments were smaller in diameter than the liners in the experiments of [1, 2], the interwire gap (about 300 μm) and the current per unit length of the circumference of the liner (about 1 MA/cm) are both fairly close to those in the experiments of [1, 2]. Accordingly, in our experiments, soft X-radiation (SXR) pulses were shorter than the current rise time by approximately the same factor (Fig. 1), the maximum achievable SXR power being 5 TW.

The plasma dynamics was experimentally visualized by laser shadowgraphy. A probing laser beam was first divided into three spatially separated rays, which were delayed with respect to each other in order to ensure probing over the desired time intervals. In experiments with laser shadowgraphy, we used liners without four “central” wires, in order to ensure the viewing of the central region of a liner through the vertical gap between the wires. These experiments were conducted with somewhat lower currents than the current in the experiment illustrated in Fig. 1. The representative laser shadowgraphs are shown in Fig. 2. We do not discuss here the pronounced axial inhomogeneity of the plasma. We draw attention to the quasi-planar plasma flows from each wire toward the liner axis. In Fig. 2, the most interesting phenomenon is the formation of a plasma prepinch (precursor) at the liner axis, which is distinctly seen in the second and third frames. These experimental results clearly indicate that the plasma flows toward the discharge axis for a relatively long time, while the liner periphery, which serves as a plasma source, remains immobile and contains most of the original liner mass.

We do not focus on the interferometric images of the plasma flows in the plane parallel to the discharge axis

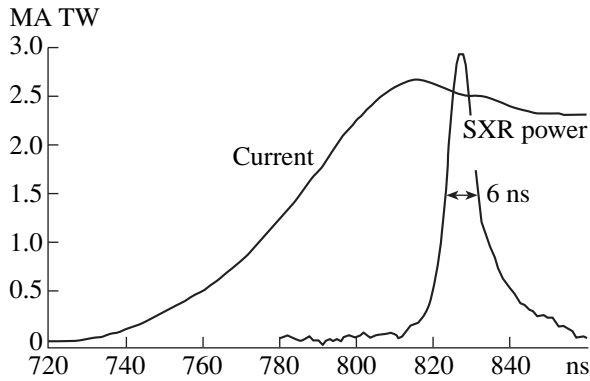


Fig. 1. Time evolutions of the SXR power and the current flowing through an 8-mm-diameter liner composed of 80 tungsten wires each having a diameter of $6\ \mu\text{m}$ (shot no. 3594).

[28]. In experiments carried out in the MAGPIE facility at the Imperial College of Science and Technology (London, UK) [8], such plasma flows were visualized by interferometric measurements along the discharge axis. Recent MHD simulations carried out by Chittenden *et al.* [12] for liners comprised of a small number of wires and treated using cylindrical geometry (the coordinates being r and ϕ) confirm the qualitative analysis that was performed about ten years ago and was briefly repeated in the previous section and also agree with the experimental data presented here.

In our experiments, prolonged plasma creation was also studied with the help of fast scanning photometry combined with X-ray frame-by-frame photography. The experimental data on an electrical discharge in an 8-mm-diameter liner composed of 32 wires each having a diameter of $10\ \mu\text{m}$ are demonstrated in Fig. 3. The upper frame of the figure presents the time evolutions of the total current and SXR intensity. The middle frame shows an optical image of the liner plasma scanned in time through a slit perpendicular to the discharge axis. The four lower frames are photos of the SXR from the liner.

Fast scanning photometry of the SXR from the liner clearly shows that the wires are immobile for a long time, while the plasma flows (in the form of narrow strips) from the wires toward the liner axis. The dynamics of the development of plasma flows is also seen in X-ray frame-by-frame photographs. The plasma is seen to fill the liner interior so that the pinch at the axis grows from the prepinch, which is maintained by the plasma inflow. The wires remain immobile for about 130 ns. The current per wire increases to 50–55 kA. Only the last X-ray photograph shows that the wires evaporate completely, although the X-ray image of the plasma is only slightly smaller in size than the original liner. At the original positions of the wires, the optical luminosity of the plasma starts to decrease 130 ns after the beginning of the current pulse. The residual plasma

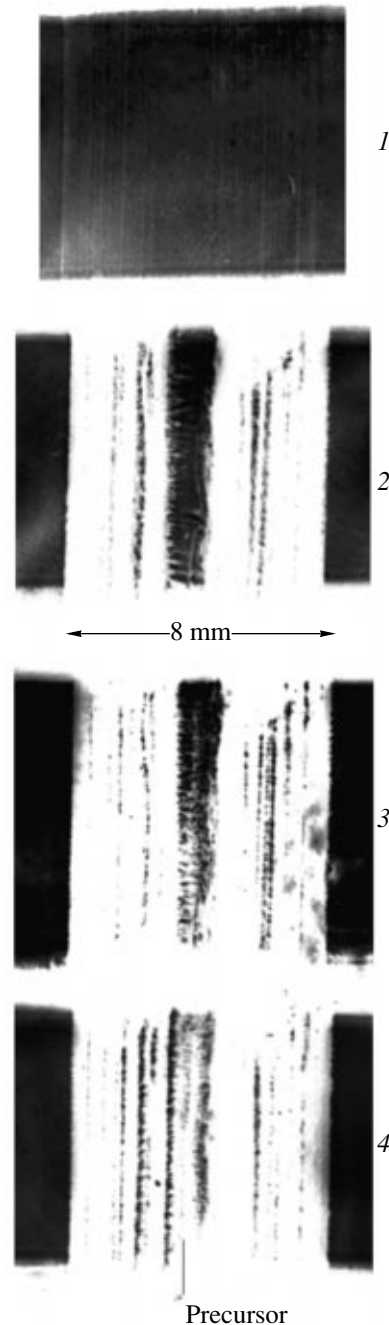


Fig. 2. Laser shadowgraphs of an 80-wire liner (shot no. 3205): (1) before the current pulse, (2) 87 ns after the beginning of the current pulse (the current per wire being 9 kA), (3) 100 ns after the beginning of the current pulse (the current per wire being 12 kA), and (4) 113 ns after the beginning of the current pulse (the current per wire being 15 kA). The prepinch (precursor) is seen to form in the central region of the initially empty diagnostic gap.

converges toward the discharge axis at a velocity of about $\sim 10^7$ cm/s.

Hence, we can conclude that the liner consists of a plasma flowing toward the axis and a dense substance,

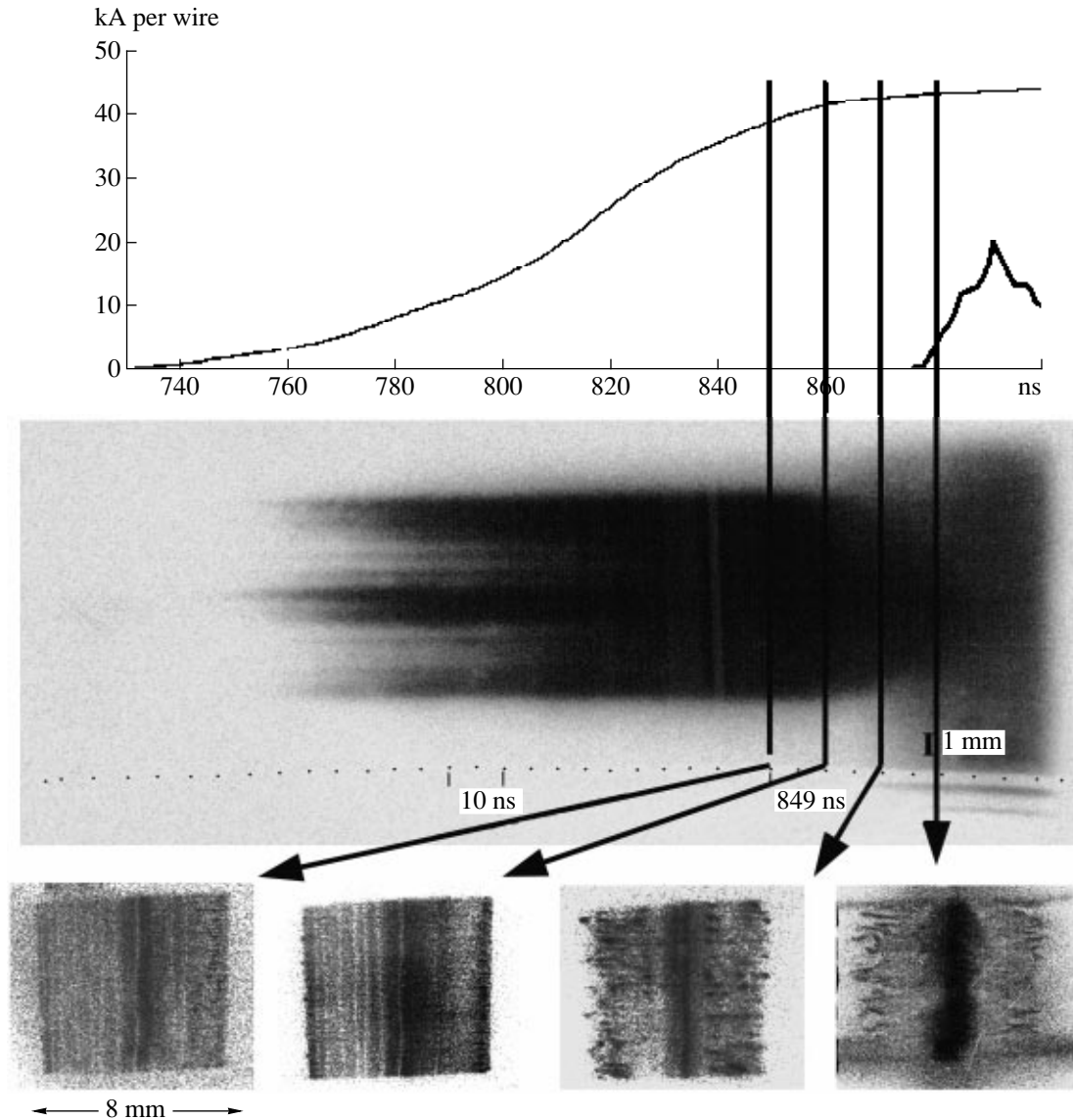


Fig. 3. Compression of a 32-wire liner (shot no. 3623).

which serves as a plasma source. This can naturally be attributed to the fact that a highly conducting plasma is produced from the substance of the exploding wires almost throughout the current pulse.

2.3. Other Examples of Liners with Prolonged Plasma Creation

Another example of heterogeneous liners with prolonged plasma creation is foam liners prepared by drying agar-agar gel [18]. A foam liner is composed of dry agar fibers and plates distributed randomly in space, the characteristic size of a spatial cell being $50\ \mu\text{m}$. Such a liner is uniform on spatial scales longer than $100\ \mu\text{m}$. An important distinctive feature of the foam liner is that the diameter of the corona that can form around each

fiber is markedly larger than the size of an elementary spatial cell. Therefore, we can assume that the skeleton of the heterogeneous liner is immersed entirely in a hot plasma. Although, at the initial discharge stages, the mass of the hot plasma is substantially smaller than the total liner mass, it carries essentially all of the discharge current, while the current carried by the cold skeleton is negligible. For this reason, the hot plasma accelerates toward the axis at a much higher rate than a liner with a uniform current distribution over mass. Although the Ampère force causes the hot plasma to converge toward the axis, the liner skeleton always remains inside the hot plasma component (in the presence of a strong axial electric field whose strength is proportional to $\approx v_r B/c$) due to prolonged plasma creation via the evaporation of the liner substance. Hence, in the experiments of [18],

a heterogeneous liner consisting of two components—a cold skeleton immersed in a hot plasma—also serves as a long-term source of hot plasma, which accelerates toward the discharge axis. The radial size of such a plasma (with a frozen-in magnetic field) can substantially exceed the skin depth.

As was noted in the Introduction, due to the cold-start effects, the gas liner also evolves into a heterogeneous structure with prolonged plasma creation.

An important feature of foam liners (as well as gas liners) is current filamentation at the initial discharge stages [18]. Presumably, the current filamentation results from the thermal-ionization instability, which occurs on spatial scales from one millimeter to fractions of a millimeter (in the azimuthal direction). However, this instability is likely to be suppressed in multiwire liners comprised of periodically spaced wires, the interwire gap (fractions of a millimeter) being of the same order as the instability scale length; at the very least, the cited papers, as well as other papers devoted to multiwire liners, contain no information on the thermal-ionization instability, which, however, may develop in liners composed of a larger number of more closely spaced wires.

3. SCENARIO OF THE EVOLUTION OF A HETEROGENEOUS LINER WITH PROLONGED PLASMA CREATION

Summarizing the above considerations, we propose the following scenario of the evolution of heterogeneous liners. As an example, we analyze a multiwire liner composed of wires that are equally spaced over a circle and are oriented perpendicular to it. Nevertheless, the proposed scenario refers to a far larger class of liners.

Heterogeneous liners are those in which, immediately after breakdown, the substance separates into two phase states—a relatively cold skeleton with a density close to that of solids and a hot plasma with a temperature of several tens of electronvolts. The cold liner skeleton always remains immersed in the hot plasma, which, however, may not form a continuous shell in the azimuthal direction. The plasma carries almost all of the discharge current and thus is Joule-heated to high temperatures. The electron heat flux and radiation flux from the hot plasma cause the cold liner skeleton to evaporate continuously. Under the action of the Ampère force, the hot plasma converges toward the discharge axis, while the massive skeleton, which carries a much smaller fraction of the total current, is almost immobile. When a portion of the hot plasma gets displaced toward the axis by a distance large enough for it not to interact with the skeleton, the processes of evaporation, ionization, and heating of the liner substance at the skeleton surface give rise to the next portion of hot plasma. We are thus dealing with the continuous creation of new portions of hot plasma, which are acceler-

ated toward the axis. At the same time, the converging hot plasma carries a frozen-in magnetic field (magnetic flux); consequently, the electric current parallel to the discharge axis flows through it. Below, we will refer to this plasma as a converging current-carrying plasma flow with a frozen-in magnetic field. The frozen-in field gives rise to plasma flow resilience. If the elements of the liner skeleton are separated by large distances, then each element gives rise to its own plasma jet accelerated toward the discharge axis. In the axial region, individual converging jets can merge into a continuous ringlike flow. This process is captured well by the two-dimensional modeling (in cylindrical r - ϕ geometry) of a multiwire liner [12]. If the skeleton elements are sufficiently close to each other, then the hot plasma forms a continuous shell around the liner skeleton. In our scenario, the difference between these two cases is not of crucial importance.

The process just described lasts until the liner skeleton evaporates completely. An important question then arises concerning the evaporation rate or the time required for the liner skeleton to evaporate completely, under the assumption that the liner mass is matched with the rise time of the current pulse in the sense that a liner with a uniform current distribution over the mass should stagnate near the discharge axis some time after the current has reached a maximum. If the hot plasma is created at a slow rate, the plasma continues to be created after the current has reached a maximum. Since the mass of the hot plasma is smaller than the matched liner mass, the portions of hot plasma that are produced at the very beginning of the pulse arrive at the discharge axis a long time before the current has reached a maximum. Thus, we are dealing with a long-term and almost steady-state hot-plasma flow from the peripheral regions where the hot plasma is continuously created toward the discharge axis. In this case, the recorded X-ray pulse from the central dense pinch is greatly smoothed and has nothing in common with the desired pulse. Otherwise, if the hot plasma is created at a very fast rate, then the plasma creation process terminates a long time before the current has reached a maximum. In this case, the plasma shell turns out to be thin in the radial direction, the frozen-in magnetic flux is far less intense, and the plasma itself is far less resilient. A further increase in the current gives rise to a magnetic piston, which leads to even stronger compression of the hot plasma into a thin shell that is rapidly destroyed due to the RT instability. This situation is analogous to a thin-walled plasma liner, which is less attractive from the standpoint of the parameters of the generated X-ray pulse. A comparison between these somewhat unfavorable limiting cases provides evidence for the existence of the optimum plasma creation rate. If the plasma production comes to an end approximately at the time when the current reaches its maximum, then the effect of the magnetic piston, which should come into play at a later time and may be dangerous due to the possible onset of the RT instability, is insignificant, the more so

because the substantial frozen-in magnetic flux makes the converging plasma flow highly resilient in the radial direction. On the other hand, by that time, a liner whose mass is matched with the current rise time is displaced toward the axis only slightly. Consequently, the thickness of the hot plasma shell can be appreciably smaller than the liner radius. Presumably, this situation provides the possibility of achieving highly compressed plasma pinches and, accordingly, generating short high-power X-ray pulses. This means that, for a liner with a matched mass, the optimum time for finishing the plasma creation process is about the time during which the current reaches its maximum.

Hence, we can see that the plasma creation rate is a key parameter for heterogeneous liners with prolonged plasma creation. It is important to investigate the plasma creation rate as a function of both the current per unit length of the liner in the azimuthal direction and the interwire gap at a prescribed surface mass density of the liner.

A comparison between the old experimental data [27] and the new results presented here and in [1, 2] clearly indicates that the plasma creation rate increases with decreasing interwire gap, the remaining parameters of the liner (in particular, its mass) being fixed, at least until the distance between the wires is larger than the transverse dimensions of the individual converging plasma jets. This important conclusion requires additional experimental and numerical verification. If this conclusion is in fact valid, then the published data from the experiments carried out by Sanford *et al.* [11] in order to investigate how the number of wires in a liner affects its dynamics might be reinterpreted in a radically different manner.

4. SIMPLEST THEORETICAL MODELS OF THE DYNAMICS OF A LINER WITH PROLONGED PLASMA CREATION

In this section, we consider the simplest theoretical models suitable for describing the dynamics of a liner with prolonged plasma creation. It is convenient to investigate the dynamic problem in two steps, i.e., to study the plasma creation process and the dynamics of the produced plasma shell separately. Although the plasma shell may have an inverse effect on plasma creation, we start by investigating the shell dynamics, assuming that the plasma source is prescribed. Moreover, in this work, we will often choose the plasma creation rate so as to satisfy the requirement that the radial structure of the plasma shell should be fairly homogeneous. We also simplify the problem under discussion by averaging over the internal spatial structure of a heterogeneous liner. This approach leads to a volume plasma source whose intensity depends only on the radius and time. The related MHD equations, which are rather difficult to find in the literature, are presented in the Appendix. Meanwhile, we begin by estimating the plasma creation rate.

4.1. Estimation of the Plasma Creation Rate

In a hot plasma flow formed by a liner with prolonged plasma creation, we can distinguish between two regions. In the first region, which is located at a large distance from the liner skeleton, the magnetic field can be assumed to be frozen in the plasma, the heat transport due to thermal conduction can be neglected, and the azimuthal structure of the heterogeneous liner is of secondary importance. In the second region, which is immediately adjacent to the skeleton of a heterogeneous liner, the above processes are important and the magnetic field is not yet frozen in the plasma. This region can naturally be called the “boundary layer,” in view of its small thickness, which is determined by the largest of the following spatial scales:

- (i) the characteristic period δ of the heterogeneous structure (e.g., the interwire gap in a multiwire liner composed of wires positioned along the generatrices of the cylinder),
- (ii) the radial thickness δ_r of the liner skeleton (e.g., the thickness of the foam liner), and
- (iii) the skin depth $\delta_s = v_m/c_A$ (where $v_m = c^2/4\pi\sigma$ is the magnetic viscosity, σ is the plasma electric conductivity, and c_A is the local Alfvén velocity).

In this section, we discuss the simplest estimate of the plasma creation rate in order to introduce the physical processes underlying plasma creation and provide at least a rough insight into the dependence of the plasma creation rate on the current flowing through the liner.

We estimate the hot-plasma creation rate \dot{m} in units of mass per unit area of the side surface of the liner, assuming that $\delta_s \gg \delta, \delta_r$. Under these conditions, we are dealing with an azimuthally homogeneous and infinitely thin plasma source. We also neglect radiation from the plasma and direct Joule heating of the cold substance of the liner skeleton. In the problem as formulated, the plasma can be produced from a relatively cold substance only via the heat flux from the hot plasma. Consequently, the plasma creation rate is determined exclusively by the heat transfer from the hot plasma toward the region immediately adjacent to the liner skeleton. Under the above assumptions, the only process responsible for such a heat transfer is electron thermal conduction. Since the hot plasma is accelerated toward the discharge axis predominantly by the Ampère force, the plasma near the source flows at a velocity close to the Alfvén velocity and the thermal component of the energy density in the plasma flow is approximately the magnetic field energy density. Thus, we have

$$v \sim c_A \sim \frac{B_0}{\sqrt{4\pi\rho}}, \quad (2)$$

$$\frac{\gamma}{\gamma-1}P \sim \frac{B_0^2}{8\pi}. \quad (3)$$

Here, v and c_A are the radial plasma velocity and characteristic Alfvén velocity in the boundary layer, respectively; the magnetic field B_0 at the outer surface of the liner is uniquely determined by the total current and liner radius; ρ and p are the typical plasma density and pressure inside the boundary layer; and γ is the adiabatic index. The left-hand side of Eq. (3) represents the specific plasma enthalpy. The numerical coefficient on the right-hand side of this equation is fairly small (about 0.1–0.2, see the next section). Nevertheless, we can use these relationships to obtain order-of-magnitude estimates and to establish the qualitative dependence of the plasma creation rate on the discharge parameters (primarily, on the discharge current).

The thickness of the boundary layer, where the magnetic field becomes frozen in the converging plasma flow, is determined by the skin depth

$$\delta_s \sim \frac{v_m}{v}. \quad (4)$$

Since, under the above simplifying assumptions, the electron thermal conduction serves as the main mechanism for heat transfer inside the boundary layer, the contribution from electron heat conduction should be comparable with the Joule heating effect:

$$\kappa \frac{T}{\delta_s^2} \sim \frac{j^2}{\sigma} \sim \frac{B_0^2}{\delta_s^2} v_m, \quad (5)$$

where T and j are the characteristic plasma temperature and electric current density in the boundary layer, respectively, and κ is the thermal conductivity.

Relationships (2)–(5) make it possible to estimate the four main parameters of the boundary layer—specifically, ρ , T , v , and δ_s —as functions of B_0 or, equivalently, the total current flowing through the liner of given radius. Assuming the Coulomb logarithms to be constant, we turn to conventional expressions for the plasma electric and thermal conductivities:

$$\sigma \propto \frac{T^{3/2}}{z}, \quad (6)$$

$$\kappa \propto \frac{T^{5/2}}{z}. \quad (7)$$

We also assume that the mean ion charge number z is a power function of temperature,

$$z \propto T^\alpha,$$

where α lies between 0 and 1, depending on the liner substance. As a result, we arrive at the following dependence of the plasma creation rate ($\dot{m} \sim \rho v$) on the total current flowing through the liner of given radius:

$$\dot{m} \propto \sqrt{AB_0^{(11-5\alpha)/(3-\alpha)}}, \quad (8)$$

where A is the atomic weight of the liner substance. We can see that, as α increases from 0 to 1, the power index

of B_0 decreases from 1.866 to 1.5. The remaining parameters of the boundary layer depend on the liner current and the atomic weight of the liner substance as follows:

$$\begin{aligned} \rho &\propto AB_0^{(5-3\alpha)/(3-\alpha)}, \quad T \propto B_0^{1/(3-\alpha)}, \\ v &\propto \sqrt{\frac{B_0^{(1+\alpha)/(3-\alpha)}}{A}}, \quad \delta_s \propto \sqrt{\frac{A}{B_0^{(4-\alpha)/(3-\alpha)}}}. \end{aligned} \quad (9)$$

Note that, according to relationships (3) and (5), the ratio of the electron gyrofrequency ω_{Be} to the electron collision frequency ν_e is on the order of unity and, in our approximation, does not depend on B_0 . This circumstance justifies the use of relationships (6) and (7), which are valid for $\omega_{Be}/\nu_e = \text{const}$. The numerical coefficients in formulas (8) and (9) will be discussed at the end of the next section.

4.2. Steady Plasma Flow near a Heterogeneous Liner with Prolonged Plasma Creation (Boundary Layer Structure)

Recall that, in a plasma flow formed by a heterogeneous liner with prolonged plasma creation, there exists a boundary layer in which an important role is played by the azimuthal liner structure and the processes of heat transport, Joule heating, and plasma diffusion transverse to the magnetic field. The boundary layer is thin enough to assume (at least, in the first approximation) that the plasma flow is steady and to neglect the cylindrical character of the flow. In contrast, in the bulk of the flow, the above processes are of secondary importance, whereas the unsteady nature of the plasma flow and its cylindrical geometry play a governing role. In this section, we completely discard the azimuthal inhomogeneity of the liner and take into account only diffusion, heat transport, and Joule heating. In other words, we treat the problem in slab geometry. In order to provide a qualitative (for the most part, analytic) consideration of the problem, we will adopt the simplest form of the equation of state and dissipative coefficients of the plasma.

The above simple estimates imply that the plasma creation rate is governed by both Joule heating and heat transport, which occur against the background of the hydrodynamic plasma flow and plasma diffusion across the magnetic field. The related set of MHD equations, which takes into account volume plasma sources, is presented in the Appendix. Disregarding the cylindrical geometry of the problem, we consider a one-dimensional planar steady plasma flow in the presence of a plasma source, which may be arbitrarily distributed in space. In this approximation, all of the quantities depend only on $x = r_L - r$ (where r_L is the outer radius of the liner) and the only nonzero components are the x -component of the plasma velocity, the y -component of the magnetic field, and the z -component of the elec-

tric field. Since the flow is steady-state, the electric field does not depend on x . Under the assumptions that the x -component of the initial momentum of the produced plasma is zero and the energy expended on creating the plasma is ensured by the heat flux from the already produced hot plasma, the steady nature of the plasma flow also implies that the momentum and energy flux densities are constant. Hence, we have

$$\rho v^2 + p + \frac{B^2}{8\pi} = \text{const} = \frac{B_0^2}{8\pi}, \quad (10)$$

$$\begin{aligned} \rho v W + \frac{1}{2}\rho v^3 - \frac{c}{4\pi}E_z B - \kappa \frac{\partial T}{\partial x} \\ = \text{const} = -\frac{c}{4\pi}E_z B_0, \end{aligned} \quad (11)$$

$$cE_z = v_m \frac{\partial B}{\partial x} - vB = \text{const}, \quad (12)$$

$$\frac{\partial}{\partial x}\rho v = q(x). \quad (13)$$

Here, v is the x -component of the plasma velocity; ρ , T , p , and W are the density, temperature, pressure, and specific enthalpy of the plasma, respectively; $q(x)$ is the intensity of the plasma source averaged over its spatial structure; κ is the thermal conductivity; $B(x)$ is the magnetic field; the magnetic field B_0 at the outer surface of the liner is uniquely determined by the total current and liner radius; and E_z is the z -component of the electric field. Consider an infinitely thin (in the radial direction) plasma source. Integrating Eq. (13) yields the relationship

$$\rho v = \text{const} = Q_m, \quad (14)$$

which is valid in the region enclosed by a cylindrical plasma source ($x > 0$), while outside of this region ($x < 0$), there is a vacuum.

Equations (10)–(12) and (14), which describe the plasma flow in the entire region enclosed by the cylindrical source ($x > 0$), should be supplemented with the boundary conditions

$$v(0) = 0, \quad T(0) = 0. \quad (15)$$

We also assume that, as $x/d \rightarrow \infty$, all of the quantities approach their finite asymptotic values, which correspond to as-yet unknown plasma parameters on the outside of the boundary layer. The second condition in (15) stems from neglecting the temperature of the cold liner skeleton in comparison with the temperature of the hot plasma. With the prescribed electric-field component E_z , which, strictly speaking, cannot be determined in this problem (see below for details), Eqs. (10)–(12) and (14) with the boundary conditions (15) have a solution only for a certain Q_m value, which is thus an eigenvalue of the problem and determines the self-consistent creation rate of the hot plasma.

In order to make the formulation of the problem as simple as possible, we turn to an elementary but quite realistic description of the plasma parameters. We represent the pressure and specific enthalpy of the plasma as $p = G\rho T$ and $W = \frac{\gamma}{\gamma-1}\frac{p}{\rho}$, where the parameter G and adiabatic index γ are both assumed to be constant. We also assume that the plasma electric conductivity σ and, accordingly, the magnetic viscosity v_m are constant and write the thermal conductivity as $\kappa = \kappa_0 T$ with $\kappa_0 = \text{const}$.

We switch to the dimensionless variables

$$\begin{aligned} B(x) &= B_0 b(\zeta), \quad E_z = -E_0 \varepsilon_z, \quad v(x) = v_0 w(\zeta), \\ \rho(x) &= \rho_0 R(\zeta), \quad T(x) = T_0 \tau(\zeta), \\ Q_m &= Q_0 \tilde{Q}, \end{aligned} \quad (16)$$

where

$$\begin{aligned} \zeta &= \frac{x}{d_0}, \quad d_0 = (8\pi)^{1/4} v_m^{3/4} \kappa_0^{1/4} G^{-1/2} B_0^{-1/2} \tilde{Q} \left(\frac{\gamma-1}{\gamma} \right)^{1/2}, \\ E_0 &= \frac{1}{(8\pi)^{1/4} c} v_m^{1/4} \kappa_0^{-1/4} G^{1/2} B_0^{3/2} \tilde{Q}^{-1} \left(\frac{\gamma}{\gamma-1} \right)^{1/2}, \\ v_0 &= \frac{1}{(8\pi)^{1/4} v_m^{1/4} \kappa_0^{-1/4} G^{1/2} B_0^{1/2} \tilde{Q}^{-1} \left(\frac{\gamma}{\gamma-1} \right)^{1/2}}, \\ \rho_0 &= (8\pi)^{-1/2} v_m^{-1/2} \kappa_0^{1/2} G^{-1} B_0 \tilde{Q}^2 \frac{\gamma-1}{\gamma}, \\ T_0 &= (8\pi)^{-1/2} \frac{\gamma}{\gamma-1} v_m^{1/2} \kappa_0^{-1/2} B_0 \tilde{Q}^{-2}, \\ Q_0 &= (8\pi)^{-3/4} ((\gamma-1)/\gamma)^{1/2} v_m^{-1/4} \kappa_0^{1/4} G^{-1/2} B_0^{3/2}, \end{aligned} \quad (17)$$

and obtain the set of equations

$$\frac{db}{d\zeta} = -\varepsilon_z + wb, \quad (18)$$

$$\frac{d\tau}{d\zeta} = \frac{\tilde{Q}^4}{\tau} \left[-2\varepsilon_z(1-b) + \tau + \frac{1}{2}w^2 \right], \quad (19)$$

$$Rw = 1, \quad (20)$$

$$w + b^2 + \frac{\gamma-1}{\gamma} R\tau = 1. \quad (21)$$

We express w and R in terms of τ and b and substitute w into Eqs. (18) and (19) to arrive at an autonomous set of differential equations for b and τ . This set of equations, supplemented with the obvious boundary conditions, constitutes an eigenvalue problem (the eigenvalue being \tilde{Q}) with the as-yet unknown parameter ε_z , which can be obtained by solving a problem on the outside of the boundary layer. Below, we consider a fairly realistic limiting case, which provides an essentially complete analytic treatment.

Before proceeding with a qualitative analysis of this limiting case, note that ε_z and γ are the only parameters that enter Eqs. (18) and (19). Therefore, the eigenvalue \tilde{Q} should be fairly close to unity (for ε_z of order unity). To within a factor on the order of unity, this circumstance, together with formulas (16) and (17), determines both the self-consistent plasma creation rate and its dependence on the liner discharge parameters—first of all, the generator current or equivalently B_0 (in our formulation of the problem).

We will use a simplifying assumption that the ionization energy required to produce both dense-liner and forerunner plasmas is substantially (by a factor of 5–10) higher than the thermal energy of the free electrons, which govern the plasma pressure. Under this assumption, we can examine the limiting case $\gamma \rightarrow 1$. In the limit of infinitely large ζ values, the left-hand side of Eq. (19) approaches zero, indicating that the specific enthalpy is on the order of the magnetic field energy $B^2/8\pi$. Since, in this limit, the plasma pressure is markedly lower (by a factor of $1/(\gamma - 1)$) than the magnetic field pressure, it can be neglected, at least, in the first approximation. In other words, on the left-hand side of Eq. (21), we can omit the term proportional to $R\tau$. As a result, Eqs. (18)–(21) become independent of the temperature and can be rewritten as

$$\frac{db}{d\zeta} = -\varepsilon_z + b(1 - b^2), \quad (22)$$

$$w = 1 - b^2, \quad (23)$$

$$R = \frac{1}{1 - b^2}. \quad (24)$$

We can see that Eq. (22) is a closed differential equation for $b(\zeta)$. The remaining parameters of the plasma flow can be expressed in terms of $b(\zeta)$ by using Eqs. (23) and (24).

The solutions to Eq. (22) with the boundary condition $w(0) = 0$ can be parameterized by the ε_z value. The condition $\varepsilon_z > 0$ corresponds to the plasma motion from the source toward the region $\zeta > 0$. The solutions with $\varepsilon_z > 2/(3\sqrt{3})$ cannot be continued through the entire region $\zeta > 0$, because, for finite ζ values, the magnetic field b approaches $-\infty$. Consequently, physically meaningful solutions to the problem of a steady plasma flow from the source are those with $0 < \varepsilon_z \leq 2/(3\sqrt{3})$. For $\zeta \rightarrow \infty$, the plasma flow velocity depends on ε_z and is determined by the condition for the right-hand side of Eq. (13) to vanish. Thus, to find the flow velocity, we must solve a cubic equation. The dependence $w(\zeta \rightarrow \infty)$ on ε_z is shown in Fig. 4. The highest flow velocity, which is reached at $\varepsilon_z = 2/(3\sqrt{3})$, is equal to the local Alfvén velocity. At lower ε_z values, the plasma flow velocity at large distances from the source is lower than the Alfvén velocity and decreases monotonically with

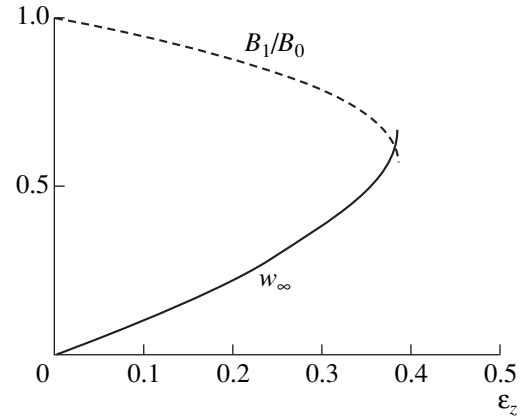


Fig. 4. Dimensionless plasma flow velocity at the inner surface of the boundary layer and the ratio of the magnetic fields at the inner surface of the boundary layer and at the outer surface of the liner as functions of the dimensionless electric field ε_z .

decreasing ε_z . The value of ε_z cannot be specified by solving the time-independent problem in slab geometry. To do this requires solving the time-dependent problem with consideration of the geometric structure of the plasma flow at large distances from the source. The plasma flow with the highest possible velocity, which can be referred to as a critical flow, occupies a special place and is the most important for our purposes. It is this solution that we are going to analyze, keeping in mind that any solution in the range $0 < \varepsilon_z < 2/(3\sqrt{3})$ is qualitatively analogous to the solution with $\varepsilon_z = 2/(3\sqrt{3})$.

To obtain the critical solution, we can integrate Eq. (22) implicitly by quadratures,

$$\zeta = \frac{b}{b - b_\infty} + \frac{1}{3} \ln \frac{(b - b_\infty)(1 + 2b_\infty)}{(b + 2b_\infty)(1 - b_\infty)} - \frac{1}{1 - b_\infty}, \quad (25)$$

in which case we have

$$b(\zeta \rightarrow \infty) = b_\infty = \frac{1}{\sqrt{3}},$$

$$w(\zeta \rightarrow \infty) = 1 - b_\infty^2 = \frac{2}{3},$$

$$R(\zeta \rightarrow \infty) = \frac{1}{1 - b_\infty^2} = 1.5,$$

$$\begin{aligned} \tau(\zeta \rightarrow \infty) &= \frac{(1 - b_\infty)(1 - b_\infty^2)(3b_\infty - 1)}{2} \\ &= \frac{2}{3} \left(\frac{2}{\sqrt{3}} - 1 \right) \approx 0.103. \end{aligned}$$

The resulting functions $b(\zeta)$, $w(\zeta)$, and $R(\zeta)$ are presented in Fig. 5. To determine the plasma temperature, we need to solve Eq. (19) with the already known w and b .

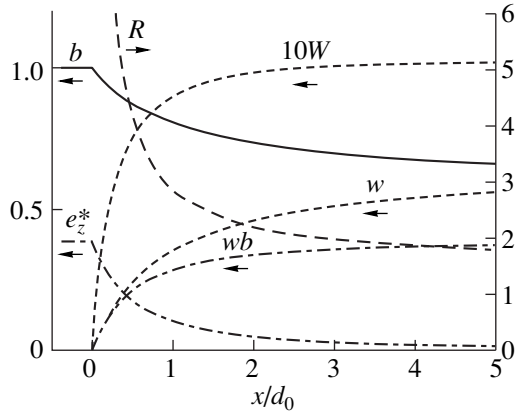


Fig. 5. Boundary layer structure near the plasma source: the dimensionless magnetic field b , plasma density R , plasma velocity w , electric (ohmic) field e_z^* in the comoving frame of reference, inductive electric field wb (in dimensional units, it is equal to vB/c), and tenfold specific plasma enthalpy W in the limit in which the adiabatic index γ tends to unity.

Solving the eigenvalue problem (19) numerically with the boundary conditions $\tau(0) = \tau(\infty) = 0$ yields

$$\tilde{Q} \approx 0.965. \quad (26)$$

The dimensionless plasma enthalpy $W(\zeta) = \tau(\zeta)$ computed in this way is also plotted in Fig. 5. In physical units, the self-consistent plasma creation rate is equal to

$$Q_m = 0.965 \sqrt[4]{\frac{\kappa_0 B_0^6 (\gamma - 1)^2}{(8\pi)^3 v_m G^2 \gamma^2}}. \quad (27)$$

Note that the dimensionless enthalpy of the plasma flow is fairly low (about 0.1). Since the dimensionless plasma pressure is even lower (e.g., at $\gamma \approx 1.2$, it is lower by a factor of approximately 5), we can see that it does not exceed several percent of the magnetic field pressure $B_0^2/8\pi$. This circumstance mostly validates the corresponding simplifying assumption.

Using the above solution to the boundary layer problem, we can rewrite Eqs. (2)–(5) in the form

$$v = \frac{B_0}{\sqrt{12\pi\rho}}, \quad \frac{\gamma}{\gamma-1} p = 0.155 \frac{B_0^2}{8\pi}, \quad (28)$$

$$\kappa T = 1.14 \times 10^{-2} \frac{B_0^2}{8\pi} v_m,$$

where v , ρ , T , and p are now the plasma parameters at the inner surface of the boundary layer. The boundary layer thickness δ corresponding to the radius at which the ohmic component of the electric field is weaker than the total electric field by a factor of approximately

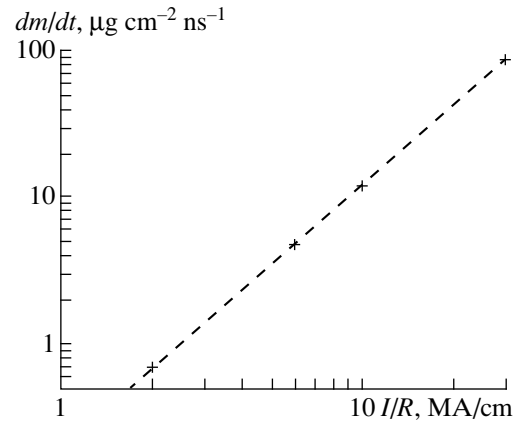


Fig. 6. Dependence of the steady-state rate at which a tungsten plasma is produced from a unit area of the side surface of the liner on the ratio of the total current flowing in the liner to its radius. The dependence was estimated from formulas (28). The calculated points (crosses) were used to obtain the power fit $\dot{m} = 0.2 \left(\frac{I[\text{MA}]}{R[\text{cm}]} \right)^{1.8} \mu\text{g cm}^{-2} \text{ns}^{-1}$ (dashed curve).

3.8 is given by the relationship

$$\delta_s = d_0 = \frac{2v_m}{3v}. \quad (29)$$

In the model adopted in this section, reducing Eqs. (2)–(5) to Eqs. (28) and (29) makes it possible to reconstruct the boundary layer parameters exactly. In more general cases, Eqs. (28) and (29) will probably give fairly good estimates.

The characteristic feature of the boundary layer structure analyzed in this section (Fig. 5) is that the heat conduction–driven energy flux starts to play an important role only in the region of sufficiently small ζ values, where the plasma still remains fairly dense and cold. Therefore, in this region, the electrons are unmagnetized, $\omega_{Be}/v_e \ll 1$, so that we are justified in using the above relationship between the electric and thermal conductivities. For this reason, when obtaining estimates, the electric and thermal conductivities in Eqs. (28) and (29) should be taken not from the general expressions, for which the adopted relationship between the thermal and electric conductivities fails to hold, but from the formulas in which the electron plasma component is assumed to be unmagnetized.

This approach was used to calculate the dependence of the rate \dot{m} at which a tungsten plasma is produced from a unit area of the side surface of the liner on the ratio of the total current flowing in the liner to its radius. The dependence illustrated in Fig. 6 was calculated under the assumption of the thermodynamically equilibrium degree of ionization of the tungsten atoms at the inner surface of the boundary layer. The expressions for the kinetic coefficients of the plasma were taken from [29]. Now, we can say that, within the accuracy

adopted in our study, this estimate of the plasma creation rate contradicts neither the experimental data from the Angara-5-1 facility nor those from the Z and Saturn facilities. The calculated plasma production rate can be estimated accurate to a numerical factor on the order of 2–3. This error stems from the simplifying assumptions made in deriving the simple formulas that describe the plasma properties; neglecting the original azimuthal structure of the liner; and neglecting the discharge axial structure, which occurs spontaneously and is distinctly seen in the photographs taken in experiments. To refine this estimate and to systematically compare it with the experimental data requires a separate study.

4.3. Numerical Simulation of the Dynamics of a Liner with a Plasma Source (Acceleration and Convergence of the Plasma Shell toward the Discharge Axis)

In this section, we report the results of the numerical simulation of the acceleration of the produced plasma shell toward the discharge axis. Here, we neglect the radial thickness of the boundary layer, whose structure was analyzed above, and/or the radial thickness of the plasma source. Accordingly, we can also ignore Joule heating, heat conduction, and plasma diffusion across the magnetic field, because these processes are only important inside the boundary layer or inside the plasma source, provided that its radial thickness is larger than that of the boundary layer. On the other hand, we systematically take into account the unsteady nature of the discharge and its cylindrical geometry. We also perform averaging over the azimuthal structure of a heterogeneous liner, assuming, e.g., that the interwire gap is smaller than the spatial resolution achievable in both the experimental investigations of the plasma flow and the present theory. Since the plasma pressure in the converging flow is lower than the magnetic field pressure (see above), we take into account only the Ampère force and discard the thermal flow parameters in the plasma shell accelerated toward the liner axis. An important feature of the problem that we are going to solve in this section is that the plasma creation rate is to be chosen so as to satisfy the conditions for the formation of the most suitable plasma shell. Thus, the problem becomes non-self-consistent. This is adopted intentionally because we do not wish to concentrate on the specific multiwire liner design for which the plasma production rate has been estimated in the previous sections. This approach makes our problem more universal.

The dynamics of the produced plasma shell can be described by the equations (see Appendix)

$$\frac{\partial}{\partial t} v + v \frac{\partial}{\partial r} v = -\frac{1}{8\pi r^2 \rho} \frac{\partial (Br)^2}{\partial r}, \quad (30)$$

$$\frac{\partial B}{\partial t} + \frac{\partial}{\partial r} v B = 0, \quad (31)$$

$$\frac{\partial \rho}{\partial t} + \frac{1}{r} \frac{\partial}{\partial r} (\rho v r) = 0. \quad (32)$$

The plasma source at the cylindrical surface $r = R_{ex}$ is incorporated into the boundary conditions as follows:

$$(\rho v)|_{r=R_{ex}} = -\dot{m}(t), \quad (33)$$

$$\left(\rho v^2 + \frac{B^2}{8\pi} \right) \Big|_{r=R_{ex}} = \frac{[B_0(t)]^2}{8\pi}, \quad (34)$$

$$-v|_{r=R_{ex}} \leq \frac{|B|}{\sqrt{4\pi\rho}} \Big|_{r=R_{ex}}. \quad (35)$$

Here, \dot{m} is the plasma creation rate (in terms of mass) near the cylindrical surface $r = R_{ex}$ per unit area of its side surface and $B_0(t) = 2I(t)/cR_{ex}$, where $I(t)$ is the total discharge current. If, in the region near the cylindrical surface $r = R_{ex}$, the plasma flow is subsonic (i.e., the flow velocity is below the Alfvén velocity), then two characteristics of the hyperbolic set of equations (30)–(32) come from this surface inward in the positive direction along the time axis. In this case, we need to impose two boundary conditions on this surface and the boundary condition (35) actually places no additional constraints. If, in this region, the flow velocity is above the Alfvén velocity, then there are three characteristics that come from this surface inward in the positive direction along the time axis. In this case, the only constraint placed by the boundary condition (35) is the fact that, in our approximation, the flow velocity in the immediate vicinity of the plasma source should be exactly equal to the Alfvén velocity, because the solution on the inside of the boundary layer (see the previous section) exists only when the flow velocity on the outside of the boundary layer is lower than or equal to the Alfvén velocity.

Equations (30)–(32) with the boundary conditions (34) and (35) and with the boundary condition $v(0, t) = 0$ at the axis were solved numerically using a modified version of the Richtmyer difference scheme (see Section 3 of Chapter V in [30]). The difference scheme was modified to keep both the mass and magnetic flux unchanged and to satisfy the radial momentum conservation law when the time step approaches zero and the spatial gradients are sufficiently high in comparison with the inverse radius. In connection with this, we note that the boundary condition (34) is a consequence of the constancy of the radial momentum flux through an infinitely thin plasma source under the assumption that the plasma is produced with zero momentum.

The results of numerical simulations carried out with

$$I(t) = I_m t^2 \frac{(3t_j - 2t)}{t_j^3} \quad (36)$$

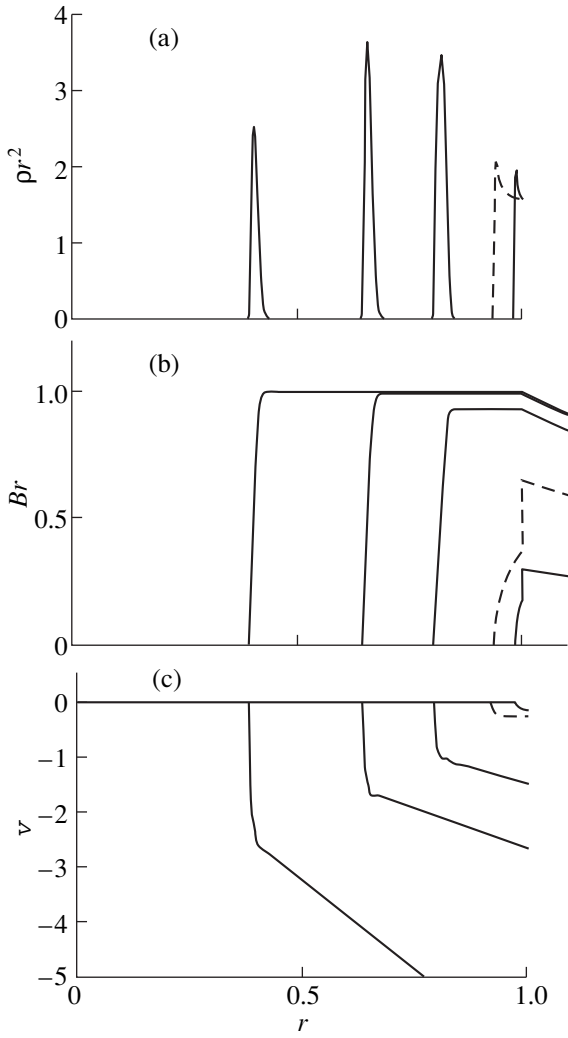


Fig. 7. Simulation of the dynamics of the plasma shell in a liner with prolonged hot-plasma creation for $t_q = 0.6t_j$; the radial profiles of (a) the plasma density multiplied by the squared radius, (b) the electric current flowing inside a cylindrical surface of radius r (i.e., the product of the magnetic field and the radius, Br), and (c) the radial plasma velocity at the times 0.36, 0.6, 0.84, 0.96, and 1.08 of the current rise time t_j . The profiles are presented in the units introduced in the text.

and

$$\dot{m}(t) = \frac{M_L}{2\pi R_{ex}} \frac{t^2(3t_j - 2t)}{t_j^3(t_j - 0.5t_q)} \theta(t_q - t), \quad (37)$$

and for different ratios $t_q/t_j = 0.6, 0.8,$ and 1 are shown in Figs. 7–9. Here, I_m is the maximum current achieved at the time $t = t_j$ after the discharge begins, M_L is the total mass per unit length of the liner, and $t = t_q$ is the time at which the plasma source ceases. In order to make the number of free parameters as small as possible, in this series of simulations, we assumed that the plasma source depletes instantaneously at the time

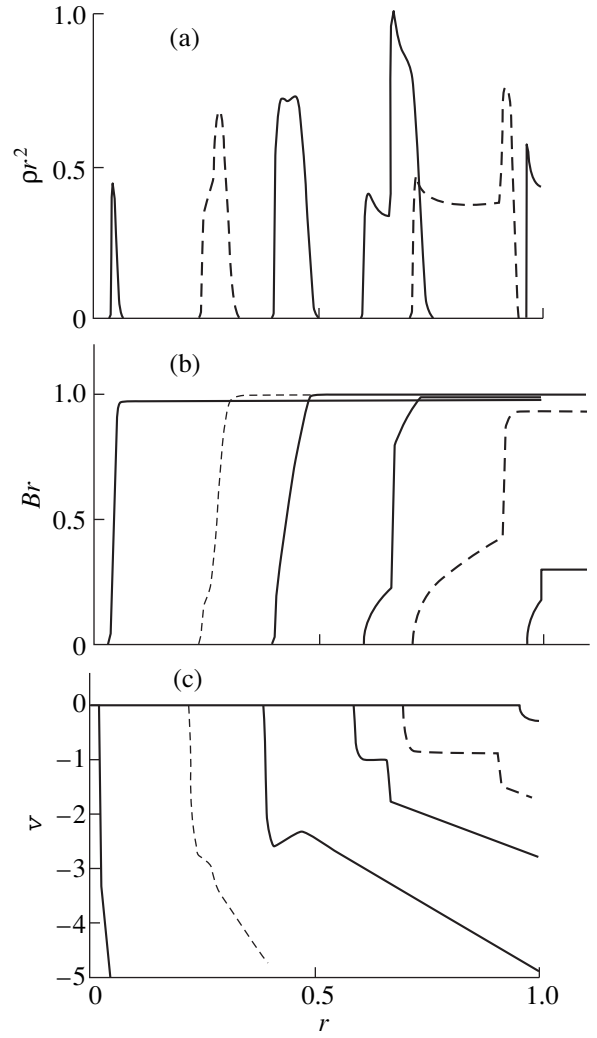


Fig. 8. Simulation of the dynamics of the plasma shell in a liner with prolonged hot-plasma creation for $t_q = 0.8t_j$; the radial profiles of (a) the plasma density multiplied by the squared radius, (b) the electric current flowing inside a cylindrical surface of radius r (i.e., the product of the magnetic field and the radius, Br), and (c) the radial plasma velocity at the times 0.36, 0.84, 0.96, 1.08, 1.14, and 1.2 of the current rise time t_j . The profiles are presented in the units introduced in the text.

when the entire cold liner substance becomes the plasma. The depletion of the plasma source was modeled using the Heaviside step function θ in Eq. (37).

The simulations described below were performed with the same liner mass, which was chosen to achieve a complete collapse at the time $t = 1.2t_j$ (in the zero-dimensional model) and was found to be $M_L \approx 0.234(I_m t_j / c R_{ex})^2$. This duration of liner compression was chosen to be close to the optimum duration, i.e., to ensure the highest efficiency of conversion of the magnetic energy of an inductive storage into the kinetic energy of the liner. We stopped the calculations at the

time $t = 1.2t_j$, i.e., before the discharge current started to fall off significantly.

The problem under consideration is a scale-invariant one. If we express the radius in units of R_{ex} , the time in units of t_j , the magnetic field in units of $2I_m/cR_{ex}$, the plasma density in units of $I_m^2 t_j^2 / (\pi c^2 R_{ex}^4)$, and the plasma velocity in units of R_{ex}/t_j , then the set of equations and the boundary conditions both rewritten in terms of these variables involve a single parameter, specifically, the ratio t_q/t_j . However, note that the solutions should also depend on the shape of the current pulse and the plasma creation rate. The profiles plotted in Figs. 7–9 were rescaled in the units introduced above.

We emphasize that the plasma source intensity was chosen to be proportional to the current throughout the current pulse. According to our test simulations, this is the case when the plasma mass is distributed most uniformly over the transverse cross section of the shell. For a weaker dependence of the plasma creation rate on the discharge current, the plasma will be concentrated near the inner boundary of the plasma shell, and, for a stronger dependence, it will accumulate near the outer boundary. It was found that, in the first case, the plasma flow velocity near the plasma source is below the Alfvén velocity, and, in the second case, it is above the Alfvén velocity. In this sense, our reference parameter values (for which, at any instant of plasma production, the plasma flow velocity at the outer boundary of the plasma flow near the plasma source is exactly equal to the Alfvén velocity) correspond to an intermediate version between these two cases. When the plasma flow velocity is equal to the Alfvén velocity, Eq. (34) shows that the plasma in the boundary layer carries a fraction of $1 - 1/\sqrt{3} \approx 42\%$ of the total discharge current.

At the time at which the source stops producing plasma (in our model, the source depletes instantaneously), the magnetic field undergoes a jump at the outer boundary of the source, thereby giving rise to a shock wave, which propagates through the forerunner plasma and converges toward the discharge axis. The shock wave, which acts to additionally compress the plasma shell to a smaller thickness, is clearly shown in Figs. 8 and 9. The effect of additional compression of the forerunner plasma is a common feature of heterogeneous liners: it occurs regardless of the rate at which the plasma production terminates. However, if this rate is sufficiently low, the additional compression is not accompanied by the onset of a shock wave.

For $t_q = 0.6t_j$, i.e., at the time when the formation of the plasma shell has come to an end, the shell itself remains essentially immobile. This situation may also be captured by a zero-dimensional model of the compression of a liner as a single entity. Consequently, for this value of the ratio t_q/t_j , the radial thickness of the produced plasma shell is very small and the compression of the shell can be described in precisely the same

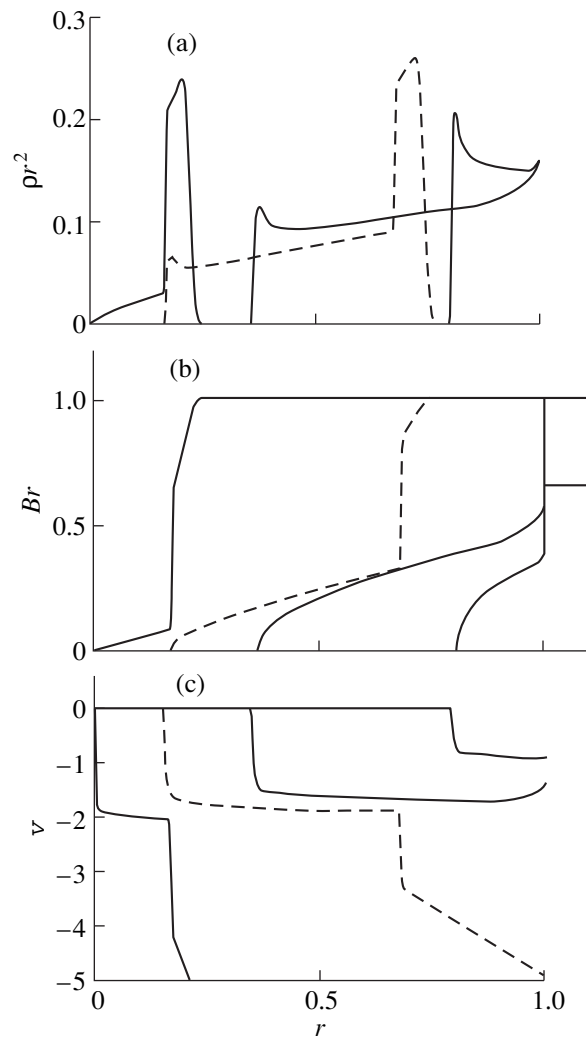


Fig. 9. Simulation of the dynamics of the plasma shell in a liner with prolonged hot-plasma creation for $t_q = t_j$; the radial profiles of (a) the plasma density multiplied by the squared radius, (b) the electric current flowing inside a cylindrical surface of radius r (i.e., the product of the magnetic field and the radius, Br), and (c) the radial plasma velocity at the times 0.6, 0.96, 1.08, and 1.2 of the current rise time t_j . The profiles are presented in the units introduced in the text.

way as in the zero-dimensional model for the compression of a thin-walled liner as a whole (Fig. 7). At first glance, it is surprising that this situation already occurs at the relatively large value $t_q/t_j = 0.6$. Such compression conditions may be favorable for the onset of strong RT instability.

For $t_q = t_j$, i.e., when the plasma production time is exactly equal to the current rise time, the leading edge of the forerunner plasma reaches the discharge axis earlier than the compression (shock) wave (Fig. 9). Consequently, the plasma shell collapses over a time insufficiently short to achieve the optimum duration of an X-ray pulse generated in the stage of collapse, when the

kinetic energy of the plasma shell and the magnetic field energy are converted into thermal energy.

Among the versions that we have simulated in this study, the version with $t_q = 0.8t_j$, which is illustrated in Fig. 8, is optimum in many aspects. By the time the source stops producing plasma, the leading edge of the forerunner plasma has traveled a distance approximately equal to 0.3 of the original liner radius. After the source is depleted, the trailing edge of the plasma shell starts to catch up with its leading edge, the radial velocity of the trailing edge being higher than that of the leading edge by a factor of approximately 2. In this stage, the plasma shell is being strongly compressed in the radial direction. The front of the compression wave reaches the leading edge of the plasma shell at the time at which the shell is at a radius about halfway between its original position and the discharge axis, the shell thickness being about 1/5 of its radius. Then, the plasma shell continues to converge toward the axis, keeping its relative thickness almost unchanged and experiencing slight radial oscillations due to the finite resilience associated with the frozen-in magnetic field. In other words, the plasma shell is compressed almost in a self-similar manner. This feature of compression will be thoroughly investigated in the next section, where we construct the related self-similar solutions. Presumably, such a plasma shell is, on the one hand, compact enough to generate a fairly short X-ray pulse when collapsing toward the discharge axis, and, on the other hand, it is sufficiently resilient and extended in the radial direction to substantially suppress its instabilities.

As was mentioned above, in order to reduce the number of free parameters of the problem, we have assumed that the plasma source depletes instantaneously and that, until this instant, the plasma production rate depends on the current only. However, in reality, the cold liner substance is depleted gradually, so that $\dot{m}(t)$ vanishes some time after it reaches its maximum. The law by which $\dot{m}(t)$ approaches zero determines the plasma distribution outside the main pinch, which forms at the system axis. In other words, the character of the source depletion process may govern the extent to which the compressed liner plasma is compact and stable.

4.4. Self-Similar Dynamics of a Thick-Walled Current-Carrying Liner Plasma with a Frozen-in Magnetic Field

The above results of the modeling of plasma shell compression in a liner with prolonged plasma creation show that, under certain conditions, the plasma shell is compressed approximately in a self-similar manner. In this section, we construct the related self-similar solution in order to illustrate that such a compression process is in fact possible. Hence, we consider the compression of the already produced plasma shell with a

frozen-in magnetic field, using a one-dimensional ideal MHD model and assuming the generator current to be constant. The corresponding equations (in a more general form) were written above [see Eqs. (30)–(32)]. We will seek their solutions with separable variables in the form

$$B(r, t) = \frac{2I}{cr_0(t)}b(\xi), \quad v_r(r, t) = \frac{r}{r_0(t)}\frac{d}{dt}r_0(t),$$

$$\rho(r, t) = \frac{\mu}{r_0^2(t)}R(\xi),$$
(38)

where

$$\xi = \frac{r}{r_0(t)},$$
(39)

and $r_0(t)$ is a characteristic time-dependent radial scale of the problem. Assuming that this scale is equal to the outer radius of the plasma shell yields the boundary conditions

$$b(1) = 1.$$
(40)

We choose the mass parameter μ to satisfy the normalization condition

$$2\pi \int_0^1 R(\xi)\xi d\xi = 1,$$
(41)

in which case μ is the total mass of the plasma shell per unit length.

On the one hand, such a solution, which actually corresponds to uniform deformation, is a generalization of the results obtained by Kulikovskii [31]. On the other hand, it extends the zero-dimensional theory of the compression of thin-walled liners (see, e.g., [32]) to the case of finite-thickness liners.

The conditions under which we can look for the desired solutions can be obtained by substituting the assumed dependences (38) and (39) into Eqs. (30)–(32):

$$\frac{1}{\xi^3 R} \frac{d}{d\xi} (b\xi)^2 = C,$$
(42)

$$r_0(t) \frac{d^2}{dt^2} r_0(t) = -\frac{I^2}{2\pi\mu c^2} C,$$
(43)

where C is a positive constant, which is determined from condition (41). We can see that the functional dependences in these solutions are specified with some freedom. Notably, the time dependence of the inner radius of the shell is in fact almost the same as that for a thin-walled liner [see Eq. (43)].

As an example, we present the solution with a piecewise constant function R , which is nonzero only over the interval $1 > \xi > \xi_1$ (Fig. 10). In this case, we have

$$R = \frac{1}{\pi(1 - \xi_1^2)}$$
(44)

for $1 > \xi > \xi_1$,

$$C = \frac{4\pi}{1 + \xi_1^2}, \quad (45)$$

$$b(\xi) = \frac{1}{\xi} \sqrt{1 - \frac{1 - \xi^4}{1 - \xi_1^4}} \quad (46)$$

and the function $r_0(t)$ satisfies the equation

$$r_0(t) \frac{d^2}{dt^2} r_0(t) = -\frac{2I^2}{\mu c^2 (1 + \xi_1^2)}. \quad (47)$$

These self-similar solutions, describing the compression of a plasma shell with a frozen-in magnetic field, show that, despite the finite thickness of the shell and its radial resilience, it is possible to achieve compact radial compression such that, in the approximation at hand, the plasma shell collapses almost instantaneously. This conclusion seems to be very important for the theory of liners with prolonged plasma creation: the finite thickness characteristic of liners with prolonged plasma creation is not, generally speaking, an obstacle to achieving very rapid conversion of the kinetic energy of a plasma shell to heat and X radiation.

4.5. Stability of a Thick-Walled Current-Carrying Liner

4.5.1. Instability of the body of the plasma shell.

In this section, we consider the acceleration-driven interchange instability of the body of the plasma shell. The next section will be aimed at an analysis of the RT instability of the outer boundary of the shell. In the stability problem, we adopt the unperturbed state that is characterized by the self-similar solutions, which were constructed in Section 4.4 and describe the compact compression of a plasma shell. The axial wavenumber k_z of perturbations remains unchanged during compression. In the geometrical-optics approximation, the short-wavelength instability of perturbations with the radial wavenumber $k_r = 0$ (and with $m = 0$ for the interchange mode) can be studied under the assumption $|k_z|(r_0 - r_1) \gg 1$. Hence, we can specify the perturbations of the plasma density, azimuthal magnetic field, and two flow velocity components v_r and v_z as

$a(t)f(\xi)e^{ik_z z}$, where $\xi = r/r_0(t)$ and the time-dependent radial scale of the problem, $r_0(t)$, was introduced above. Because of the magnetic field-induced resilience of the plasma shell, the perturbations under consideration (specifically, those with frequencies much lower than $k_z c_A$) should not disturb the magnetic field. In other words, the perturbed magnetic field in such relatively slow perturbations can be neglected in our approximation. On the other hand, since the magnetic field is frozen in the plasma, the quantity $B/\rho r$ should be constant along the streamlines of the plasma flow. Consequently,

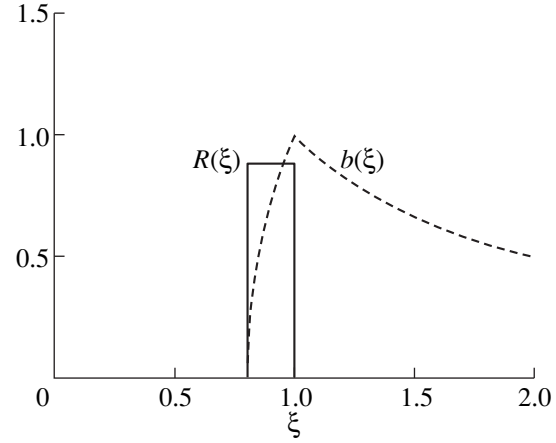


Fig. 10. Radial profiles of the dimensionless plasma density $R(\xi)$ and the dimensionless magnetic field in a plasma shell converging in a self-similar manner for a piecewise constant density, which is nonzero within the interval $1 > \xi > \xi_1 = 0.8$.

the perturbed plasma density $\tilde{\rho}$ and perturbed radial flow velocity \tilde{v}_r are related by the equation

$$-\frac{d}{dt} \frac{\tilde{\rho} B}{\rho^2 r} + \tilde{v}_r \frac{\partial}{\partial r} \frac{B}{\rho r} = 0, \quad (48)$$

which follows from the continuity and frozen-in conditions. Here, the unperturbed quantities, namely, those that are not identified by a tilde, refer to the self-similar solutions constructed in the previous section. For instance, the total plasma density is equal to $\rho + \tilde{\rho}$. The derivative $d/dt = \partial/\partial t + v_r \partial/\partial r$ corresponds to the Lagrange derivative along the unperturbed trajectories of the volume elements of the plasma. Recall that the unperturbed plasma parameters are z -independent. From Eq. (48), we obtain

$$\frac{d}{dt} \frac{\tilde{\rho}}{\rho} = -\tilde{v}_r \frac{\partial}{\partial r} \ln \frac{B}{\rho r}. \quad (49)$$

Linearizing the Euler equation for the radial flow velocity component yields

$$\frac{d}{dt} \tilde{v}_r + \tilde{v}_r \frac{\partial}{\partial r} v_r = \frac{\tilde{\rho}}{\rho} \frac{B}{4\pi \rho r} \frac{\partial (Br)}{\partial r} = -\frac{\tilde{\rho}}{\rho} \xi \frac{d^2}{dt^2} r_0(t) \quad (50)$$

or, equivalently,

$$\frac{1}{r_0} \frac{d}{dt} r_0 \tilde{v}_r = -\frac{\tilde{\rho}}{\rho} \xi \frac{d^2}{dt^2} r_0. \quad (51)$$

Equations (49) and (51) can be reduced to the following second-order linear differential equation for the relative perturbed plasma density:

$$\frac{d}{dt} r_0^2 \frac{d}{dt} \frac{\tilde{\rho}}{\rho} = -\frac{\tilde{\rho}}{\rho} \frac{\partial \ln(B/\rho r)}{\partial \ln \xi} r_0 \frac{d^2}{dt^2} r_0, \quad (52)$$

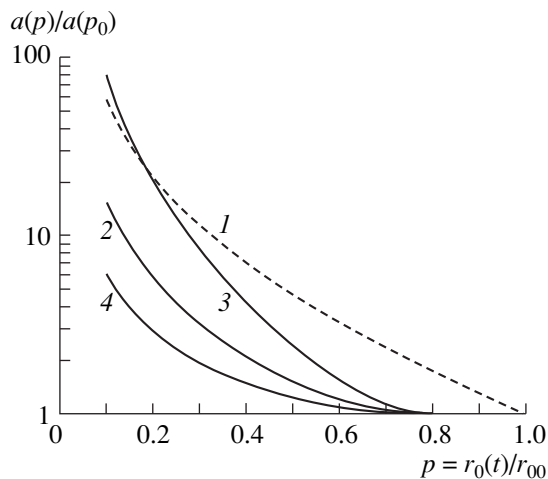


Fig. 11. Growth of the relative density perturbations during compression for (1) $K = 1.8$ and $p_0 = 1$, (2) $K = 1.8$ and $p_0 = 0.8$, (3) $K = 4.3$ and $p_0 = 0.8$, and (4) $K = 1$ and $p_0 = 0.8$. Profiles 1 and 2 correspond to a plasma shell whose radial thickness is about 1/5 of its radius.

where, by virtue of Eq. (43), we have

$$r_0 \frac{d^2}{dt^2} r_0 = -\frac{I^2 C}{2\pi\mu c^2}. \quad (53)$$

We denote the radius at which the derivative $dr_0(t)/dt$ vanishes by r_{00} and pass over from the time t to the new variable $p(t) = r_0(t)/r_{00}$, which has the meaning of the time-dependent degree of compression of the plasma shell. Then, we arrive at the following equation for the amplitude $a(p, \xi)$ of the relative density perturbations:

$$\sqrt{\ln \frac{1}{p} \frac{d}{dp} p^2} \sqrt{\ln \frac{1}{p} \frac{d}{dp} a} = \frac{1}{2} a \frac{\partial \ln(B/\rho r)}{\partial \ln \xi}. \quad (54)$$

As was noted above, the frozen-in condition implies that the factor $\partial \ln(B/\rho r)/\partial \ln \xi$ on the right-hand side of this equation is actually dependent only on ξ . We can see that, for

$$\frac{\partial \ln(B/\rho r)}{\partial \ln \xi} = \frac{\partial \ln(B/\rho r)}{\partial \ln r} > 0 \quad (55)$$

the perturbation amplitude increases during compression. According to Eq. (54), the characteristic time required for the instability to develop is proportional to the square root of the shell thickness. From this point of view, thicker plasma shells are more preferable.

To be specific, let us turn to self-similar compression and consider how the perturbations grow in the vicinity of a cylindrical surface of radius $\xi = \sqrt{(1 + \xi_1^2)}/2$, which divides the plasma shell into two parts of equal mass, assuming the rectangular plasma-density profile [see formulas (44)–(47)]. We treat the case $\xi_1 = 0.8$, because this ξ_1 value corresponds to the relative shell thickness, which was calculated for

$t_q = 0.8t_j$ in Section 4.4 and for which the radial thickness of a completely compressed shell (after the plasma creation process terminates) is about 1/5 of its radius. In this case, the coefficient $K = (1/2)\partial \ln(B/\rho r)/\partial \ln \xi$ on the right-hand side of Eq. (54) is approximately equal to 1.8. We also present some other values of this coefficient for other values of ξ : $K(\xi_1 = 0.7) \approx 0.76$, $K(\xi_1 = 0.85) \approx 2.4$, and $K(\xi_1 = 0.9) \approx 4$. Equation (54) was solved numerically with the initial condition $\tilde{v}_r(p = p_0) = 0$. We calculated the amplification coefficient of the relative amplitude $a(p)/a(p_0)$ of the density perturbations for $p < p_0$. For $K \approx 1.8$ and $p_0 = 1$, the amplification coefficient is shown by the dashed curve in Fig. 11. One can see that, by the time when the original liner is compressed tenfold, the seed perturbation amplitude increases by a factor of about 100. However, we stress that, according to the results from numerical simulations of the compression of a plasma shell in a liner with prolonged plasma creation (Fig. 8), the radial shell thickness at the time when the cold liner substance has been completely evaporated is still appreciably larger than that after the compression by the shock wave (and, accordingly, the gradient $B/\rho r$ is appreciably smaller than the final one). That is why, before compression, the instability is suppressed to a markedly greater extent than after the compression by the shock wave. Consequently, it is more expedient to choose $p_0 = 0.8$. By almost the same time, the front of the compression wave reaches the middle of the shell. The profiles displayed in Fig. 11 were obtained precisely for $p_0 = 0.8$ and for the three parameter values $K = 0.76, 1.6,$ and 4 , for which the relative radial thickness of the plasma shell equals 1/3, 1/5, and 1/10, respectively.

Hence, when the plasma creation process terminates at a time equal to 0.8 of the current rise time (in which case the thickness of the shell after the compression by the shock wave will be approximately equal to 1/5 of its radius), the relative amplitude of the seed density perturbations increases (due to the internal interchange instability) by a factor of about 20 by the time the original liner is compressed nearly tenfold. This result allows us to hope that seed perturbations with relative amplitudes of no more than 5% will not destroy the plasma shell as it is compressed tenfold. This rough analysis was performed under the assumption that, before the cold liner substance evaporates completely, the plasma creation rate is proportional to the current flowing through the liner, in which case the mass of the plasma shell is fairly uniformly distributed over its transverse cross section. A weaker or stronger dependence of the plasma creation rate on the total current will cause the plasma to be concentrated either near the leading or trailing edge of the plasma shell, so that the role played by the internal interchange instability may become more important.

4.5.2. Role of the instability of the outer boundary of the shell. While the body of the plasma shell is subject to interchange instability, which was analyzed

in the previous section, the outer boundary of the shell may experience conventional RT instability [33].

The compression under discussion differs from ordinary liner compression in that, before the plasma creation process has come to an end, the outer boundary of the plasma shell is not a freely moving boundary, because it is attached to the immobile cold dense liner skeleton. The liner skeleton is in turn immobile because it carries a small fraction of the total current. Just after the plasma source stops producing plasma (provided that the final stage of plasma production is sufficiently short), the fraction of the total current that flowed through the boundary layer when the plasma was still being produced and then accelerated the plasma to the Alfvén velocity gives rise to a converging compression wave, which starts to propagate through the plasma flow. Before the compression wave reaches the leading edge of the plasma flow, the plasma is accelerated only at the front of the compression wave, while the plasma behind the front converges with an almost constant velocity. Consequently, before the compression wave reaches the leading edge, the ordinary RT instability cannot occur, which indicates that the compression of the outer boundary of a light liner with prolonged plasma creation is more stable in comparison with what is usually expected.

Another distinctive feature of the compression process under discussion is that the plasma shell is fairly thick because of its resilience associated with the frozen-in magnetic field. For this reason, the time required for the RT instability to destroy such a shell is fairly long. The results of recent ICF-related theoretical and experimental investigations of the RT instability (see, e.g., [34–36]) show that, during the development of the three-dimensional RT instability on scale lengths comparable with the thickness of a thin plasma shell, the distance that the accelerated shell can travel is roughly seven times its thicknesses (provided that there are no additional stabilizing factors). Since the liner under consideration is accelerated under the action of the magnetic field, the development of the RT instability is partially suppressed in one direction due to the anisotropy of the instability. For this reason, the plasma shell accelerated by the magnetic field is presumably somewhat more stable than that accelerated by the pressure of a light gas.

Hence, we can suppose that the plasma shell with a frozen-in magnetic field and with a thickness of about 1/5 of its radius can be successfully compressed (without complete destruction) to a radius of about 1/10 of the original liner radius. We speak of self-similar compression, which was considered at the beginning of this section. Achieving such a stable compression of thinner plasma shells may turn out to be problematic.

Summing up the results of our study of the instabilities of a compressed plasma shell, we can say that the plasma shell formed during prolonged plasma creation can be compressed fairly efficiently under the condi-

tions that the plasma creation rate is approximately proportional to the total current, the cold liner substance evaporates completely some time before the current reaches its maximum, and the plasma compression comes to an end some time after the current reaches its maximum. After the beginning of the current pulse, the plasma creation process should optimally terminate at a time equal to 0.8–0.9 of the current rise time, the compression time being 1.2 times as long as the current rise time.

5. CONCLUSION

We have shown that, in high-current high-voltage facilities, multiwire, foam, and even gas liners are characterized by prolonged plasma creation, which can last almost throughout the current pulse. The Ampère force causes the rarefied hot plasma produced to converge toward the liner axis, giving rise to the radial plasma flow, while the liner skeleton, which carries a small fraction of the total current, is almost immobile. This phenomenon is independent of whether or not the produced hot plasma forms a continuous shell in the azimuthal direction. This can result in the formation of a fairly thick current-carrying plasma shell with a frozen-in magnetic field, the shell thickness being much larger than the skin depth. We have studied the main factors that govern the rate at which the hot plasma is produced. We have developed the simplest theoretical model, which allows us to estimate the plasma creation rate and to analyze the structure of the boundary layer near the plasma source.

A thick current-carrying plasma shell with a frozen-in magnetic field is characterized by a certain resilience, which makes liner compression more stable against the RT instability in comparison with plasma liners whose thickness is about the skin depth and which are accelerated by a magnetic piston. We have constructed self-similar solutions and have simulated the dynamics of a plasma shell formed by a liner with prolonged plasma creation in order to show that fairly thick shells can also be compressed into a very compact pinch at the device axis. This conclusion rejects the widely accepted objection that the compact compression of such a plasma shell is unlikely to be achieved. The main obstacles that may hamper compact compression are the high plasma pressure in the shell and plasma instabilities. For the liners under consideration, both of these obstacles are avoided by composing the liners of chemical elements that are heavy enough for the plasma creation process to terminate a short time before the current reaches its maximum, the liner mass being such that the plasma shell is compressed completely some time after the current reaches its maximum. Under the assumption that the plasma creation rate is proportional to the total discharge current until the plasma source is depleted, we have shown that the optimum time for the complete evaporation of the cold liner is approximately equal to 0.8 of the current rise

time, the compression time being approximately equal to 1.2 of the current rise time. After the plasma source ceases, additional compression makes it possible to achieve a plasma shell with a thickness of about 1/5 of its radius, thereby facilitating further fairly stable collapsing of the liner.

Presumably, the authors of [1, 2] grasped the experimental way to achieve the optimum parameter range for the assumed design of multiwire liners, namely, liners composed of identical wires placed along the generatrices of a cylinder with a given radius. According to our simple estimates, for a very narrow interwire gap, such a multiwire liner design leads to a stronger dependence of the plasma production rate on the current than desired. We think that this fact opens new possibilities for refining the already obtained results by making the liner design more complicated in order to further optimize the time dependence of the plasma creation rate.

Production of a new plasma at the discharge periphery (or, more precisely, at the inner surface of the insulator) also occurs in explosion magnetic generators. There are publications on this subject (see [37] and the literature cited therein) in which the density of the plasma flow from the insulator into the discharge chamber is estimated. Under these conditions, the radiative energy transfer toward the insulator surface is of great importance. In [37], the value of \dot{m} was estimated for a Plexiglass insulator with allowance for the above effect, but without taking into account electron heat conduction. In our notation, this estimate takes the form $\dot{m} = 0.17(I[\text{MA}]/R[\text{cm}])^{1.7} \mu\text{g cm}^{-2} \text{ns}^{-1}$. This formula may be compared with the result obtained in Section 4.2 for tungsten (see Fig. 6). The fact that these formulas, which were obtained under very different assumptions, are similar speaks well for their reliability.

ACKNOWLEDGMENTS

We are grateful to S.V. Bulanov, S.V. Zakharov, and I.V. Glazyrin for fruitful discussions. This work was supported in part by the Russian Foundation for Basic Research, project nos. 99-02-17952, 99-02-16471, and 00-02-16177.

APPENDIX

Set of Equations for a Cylindrical MHD Problem with a Plasma Source

In the absence of an axial magnetic field, cylindrically symmetric plasma flows with spatially averaged plasma-source terms are described by the following set of modified MHD equations:

$$\frac{\partial}{\partial t} \rho v + \frac{1}{r} \frac{\partial}{\partial r} \rho v^2 r = -\frac{\partial p}{\partial r} - \frac{1}{c} j B, \quad (\text{A.1})$$

$$\frac{\partial B}{\partial t} + \frac{\partial}{\partial r} v B = c \frac{\partial}{\partial r} \left(\frac{j}{\sigma} \right), \quad (\text{A.2})$$

$$\frac{\partial \rho}{\partial t} + \frac{1}{r} \frac{\partial}{\partial r} (\rho v r) = q(r, t), \quad (\text{A.3})$$

$$\frac{\partial}{\partial t} \rho \varepsilon_e + \frac{1}{r} \frac{\partial}{\partial r} \rho \varepsilon_e v r + \frac{p_e}{r} \frac{\partial}{\partial r} v r$$

$$= -\frac{1}{r} \frac{\partial}{\partial r} r q_{Te} + \frac{j^2}{\sigma} + C_{ei}(T_i - T_e) - Q_r, \quad (\text{A.4})$$

$$\frac{\partial}{\partial t} \rho \varepsilon_i + \frac{1}{r} \frac{\partial}{\partial r} \rho \varepsilon_i v r + \frac{p_i}{r} \frac{\partial}{\partial r} v r$$

$$= -\frac{1}{r} \frac{\partial}{\partial r} r q_{Ti} - C_{ei}(T_i - T_e) + \frac{v^2}{2} q(r, t) \quad (\text{A.5})$$

or by the set

$$\rho \frac{d}{dt} v = -\frac{\partial p}{\partial t} - \frac{1}{c} j B - v q(r, t), \quad (\text{A.6})$$

$$\frac{\partial B}{\partial t} + \frac{\partial}{\partial r} v B = c \frac{\partial}{\partial r} \left(\frac{j}{\sigma} \right), \quad (\text{A.7})$$

$$\frac{\partial \rho}{\partial t} + \frac{1}{r} \frac{\partial}{\partial r} (\rho v r) = q(r, t), \quad (\text{A.8})$$

$$\rho \frac{d}{dt} \varepsilon_e + \frac{p_e}{\rho} \frac{\partial}{\partial r} v r = -\frac{1}{r} \frac{\partial}{\partial r} r q_{Te} + \frac{j^2}{\sigma}$$

$$+ C_{ei}(T_i - T_e) - Q_r - \rho \varepsilon_e q(r, t), \quad (\text{A.9})$$

$$\rho \frac{d}{dt} \varepsilon_i + \frac{p_i}{r} \frac{\partial}{\partial r} v r = -\frac{1}{r} \frac{\partial}{\partial r} r q_{Ti}$$

$$- C_{ei}(T_i - T_e) + \left(\frac{v^2}{2} - \varepsilon_i \right) \rho q(r, t). \quad (\text{A.10})$$

Here, ρ is the plasma density; v is the radial component of the plasma velocity; B is the azimuthal component of the magnetic field; j is the axial component of the electric current density,

$$j = \frac{c}{4\pi} \frac{1}{r} \frac{\partial}{\partial r} B r, \quad (\text{A.11})$$

$T_{e,i}$ are the electron and ion plasma temperatures; $p_{e,i}$ are the electron and ion pressures; $\varepsilon_{e,i}$ are the specific energies (per unit mass) of the electrons and ions; r is the radial coordinate; and $d/dt = \partial/\partial t + v\partial/\partial r$. The modified MHD equations are supplemented with the simplified Ohm's law for the axial component of the electric field, $E = -\frac{1}{c} v B + \frac{j}{\sigma}$, and with the simplified expressions for the electron and ion heat fluxes,

$$q_{Te,i} = -\kappa_{e,i} \frac{\partial T_{e,i}}{\partial r}. \quad (\text{A.12})$$

The continuity equations (A.3) and (A.8) incorporate the plasma source intensity. The plasma is assumed to be created with a zero momentum exclusively at the expense of the energy of the plasma already produced.

Otherwise, the right-hand sides of Eqs. (A.1), (A.4), and (A.5) should be supplemented with the corresponding source terms. It is assumed that $p_{e,i}$, $\epsilon_{e,i}$, $\kappa_{e,i}$, C_{ei} , and σ are functions only of ρ , T_e , and T_i ; and that $\kappa_{e,i}$ and σ also depend on $|B|$. In the above equations, the effects of viscosity are discarded, because they are most likely of secondary importance in the problem under study.

Many problems can be solved by assuming $q = 0$ and by incorporating the plasma source only into the boundary conditions. Notably, if the radius of the plasma source is much larger than its radial thickness, then integrating Eq. (A.1) over the radius shows that the quantity $\rho v^2 + p + B^2/8\pi$ is continuous at the cylindrical surface corresponding to the source.

REFERENCES

1. T. W. L. Sanford, G. O. Allshouse, B. M. Marder, *et al.*, Phys. Rev. Lett. **77**, 5063 (1996).
2. R. B. Spielman, C. Deeney, G. A. Chandler, *et al.*, Phys. Plasmas **5**, 2105 (1998).
3. V. P. Smirnov, E. V. Grabovskii, V. I. Zaitsev, *et al.*, in *Proceedings of the 8th International Conference on High-Power Particle Beams (BEAMS-90)*, Novosibirsk, 1990, Ed. by B. N. Breizman and B. A. Knyazev (World Scientific, Singapore, 1991), Vol. 1, p. 61.
4. C. Deeney, P. D. LePell, T. Nash, *et al.*, in *Proceedings of the 9th International Conference on High-Power Particle Beams (BEAMS-92)*, Washington, 1992, Ed. by D. Mosher and G. Cooperstein (NTIS, Springfield, 1992), Vol. 1, p. 159.
5. A. V. Branitskii, V. D. Vikharev, S. V. Zakharov, *et al.*, Fiz. Plazmy **17**, 531 (1991) [Sov. J. Plasma Phys. **17**, 311 (1991)].
6. M. G. Haines, IEEE Trans. Plasma Sci. **26**, 1275 (1998).
7. S. V. Lebedev, R. Aliaga-Rossel, J. P. Chittenden, *et al.*, Phys. Plasmas **5**, 3366 (1998).
8. S. V. Lebedev, I. H. Mitchell, R. Aliaga-Rossel, *et al.*, Phys. Rev. Lett. **81**, 4152 (1998).
9. B. M. Marder, T. W. L. Sanford, and G. O. Allshouse, Phys. Plasmas **5**, 2997 (1998).
10. T. W. Sanford, R. C. Mock, R. B. Spielman, *et al.*, Phys. Plasmas **5**, 3737 (1998).
11. T. W. Sanford, R. C. Mock, T. J. Nash, *et al.*, Phys. Plasmas **6**, 1270 (1999).
12. J. P. Chittenden, S. V. Lebedev, A. R. Bell, *et al.*, Phys. Rev. Lett. **83**, 100 (1999).
13. R. Benattar, S. V. Zakharov, A. F. Nikiforov, *et al.*, Phys. Plasmas **6**, 175 (1999).
14. V. V. Branitskii, E. V. Grabovskii, I. N. Frolov, *et al.*, in *Proceedings of 12th International Conference on High-Power Particle Beams (BEAMS-98)*, Haifa, 1998, Ed. by M. Makkovits and J. Shilon (Rafael, Haifa, 1998), Vol. 2, p. 599.
15. A. V. Batyunin, A. N. Bulatov, V. D. Vikharev, *et al.*, Fiz. Plazmy **16**, 1029 (1990) [Sov. J. Plasma Phys. **16**, 597 (1990)].
16. A. V. Branitskii, S. A. Dan'ko, A. V. Gerasov, *et al.*, Fiz. Plazmy **22**, 307 (1996) [Plasma Phys. Rep. **22**, 277 (1996)].
17. I. K. Aivazov, M. B. Bekhtev, V. V. Bulan, *et al.*, Fiz. Plazmy **16**, 645 (1990) [Sov. J. Plasma Phys. **16**, 373 (1990)].
18. A. V. Branitskii, E. V. Grabovskii, M. V. Zurin, *et al.*, Fiz. Plazmy **25**, 1060 (1999) [Plasma Phys. Rep. **25**, 976 (1999)].
19. D. L. Peterson, R. R. Bower, K. D. McLenithan, *et al.*, Phys. Plasmas **5**, 3302 (1998).
20. L. E. Aranchuk, S. L. Bogolyubskii, G. S. Volkov, *et al.*, Fiz. Plazmy **12**, 1324 (1986) [Sov. J. Plasma Phys. **12**, 765 (1986)].
21. N. A. Bobrova, T. L. Razinkova, and P. V. Sasorov, Fiz. Plazmy **14**, 1053 (1988) [Sov. J. Plasma Phys. **14**, 617 (1988)].
22. J. D. Sethian, A. E. Robson, K. A. Gerber, and A. W. DeSilva, Phys. Rev. Lett. **59**, 892, 1790 (1987).
23. I. R. Lindemuth, G. H. McCall, and R. A. Nobel, Phys. Rev. Lett. **62**, 264 (1989); P. Shehey, J. Hammel, and I. R. Lindemuth, Phys. Fluids B **4**, 3698 (1992).
24. N. A. Bobrova, T. L. Razinkova, and P. V. Sasorov, Fiz. Plazmy **18**, 517 (1992) [Sov. J. Plasma Phys. **18**, 269 (1992)].
25. N. A. Bobrova, V. V. Neudachin, T. L. Razinkova, and P. V. Sasorov, in *Proceedings of the 3rd International Conference, London, 1993*, Ed. by M. Haines and A. Knight (AIP, New York, 1994), p. 10.
26. C. Stallings, K. Childers, I. Roth, *et al.*, Appl. Phys. Lett. **29**, 404 (1976); F. Burkhalter, J. Davis, J. Rauch, *et al.*, J. Appl. Phys. **50**, 705 (1979).
27. M. V. Bekhtev, V. L. Vikharev, S. V. Zakharov, *et al.*, Zh. Éksp. Teor. Fiz. **95**, 1653 (1989) [Sov. Phys. JETP **68**, 955 (1989)]; I. K. Aivazov, V. D. Vikharev, G. S. Volkov, *et al.*, Fiz. Plazmy **14**, 197 (1988) [Sov. J. Plasma Phys. **14**, 110 (1988)].
28. V. V. Alexandrov, A. V. Branitskii, G. S. Volkov, *et al.*, in *Proceedings of 1st International Conference on Inertial Fusion Sciences and Application (IFSA-99)*, Bordeaux, 1999, Ed. by C. Labaune, W. J. Hogan, and K. A. Tanaka (Elsevier, Paris, 1999), p. 591.
29. N. A. Bobrova and P. V. Sasorov, Fiz. Plazmy **19**, 789 (1993) [Plasma Phys. Rep. **19**, 409 (1993)].
30. R. D. Richtmyer, *Difference Methods for Initial-Value Problems* (Interscience, New York, 1957; Inostrannaya Literatura, Moscow, 1960).
31. A. G. Kulikovskii, Dokl. Akad. Nauk SSSR **114**, 984 (1957) [Sov. Phys. Dokl. **2**, 269 (1958)]; F. S. Felber, Phys. Fluids **25**, 643 (1982).
32. L. A. Artsimovich, *Controlled Thermonuclear Reactions*, Ed. by A. Kolb and R. S. Pease (Fizmatgiz, Moscow, 1961; Gordon and Breach, New York, 1964).
33. N. F. Roderic, T. W. Hussey, R. J. Faehl, and R. W. Boyd, Appl. Phys. Lett. **32**, 273 (1978).
34. D. L. Youngs, Physica D (Amsterdam) **12**, 32 (1984).
35. K. I. Read, Physica D (Amsterdam) **12**, 45 (1984).
36. M. M. Basko, Phys. Plasmas **1**, 1270 (1994).
37. S. F. Garanin, E. S. Pavlovskii, and V. B. Yakubov, Prikl. Mekh. Tekh. Fiz., Nos. 2, 9 (1984).

Translated by G. V. Shepekina